Phase space analysis of sign-shifting interacting dark energy models

Sudip Halder,[1,*] Jaume de Haro,[2,†] Tapan Saha,[1,‡] and Supriya Pan[1,3,§]

[1]*Department of Mathematics, Presidency University, 86/1 College Street, Kolkata 700073, India*
[2]*Departament de Matemàtiques, Universitat Politècnica de Catalunya, Diagonal 647, 08028 Barcelona, Spain*
[3]*Institute of Systems Science, Durban University of Technology, P.O. Box 1334, Durban 4000, Republic of South Africa*

(Received 17 October 2023; accepted 1 March 2024; published 16 April 2024)

The theory of nongravitational interaction between a pressureless dark matter (DM) and dark energy (DE) is a phenomenologically rich cosmological domain which has received magnificent attention in the community. In the present article we have considered some interacting scenarios with some novel features: the interaction functions do not depend on the external parameters of the Universe, rather, they depend on the intrinsic nature of the dark components; the assumption of unidirectional flow of energy between DM and DE has been extended by allowing the possibility of bidirectional energy flow characterized by some sign shifting interaction functions; and the DE equation of state has been considered to be either constant or dynamical in nature. These altogether add new ingredients in this context, and we performed the phase space analysis of each interacting scenario in order to understand their global behavior. According to the existing records in the literature, this combined picture has not been reported elsewhere. From the analyses, we observed that the DE equation of state as well as the coupling parameter(s) of the interaction models can significantly affect the nature of the critical points. It has been found that within these proposed sign shifting interacting scenarios it is possible to obtain stable late time attractors, which may act as global attractors corresponding to an accelerating expansion of the Universe. The overall outcomes of this study clearly highlight that the sign shifting interaction functions are quite appealing in the context of cosmological dynamics, and they deserve further attention.

DOI: 10.1103/PhysRevD.109.083522

I. INTRODUCTION

Over the last two decades, dynamics of the Universe have been surprisingly thrilling due to the availability of a large amount of observational data. At the end of the 1990s, observations from type Ia supernovae first reported that our Universe is passing through a phase of accelerated expansion [1,2], and this accelerated expansion is supposed to be driven by the presence of some exotic matter sector in our Universe sector having large negative pressure. This exotic matter can be described in various ways. Two well-known approaches are the modification of the matter sector of the Universe in the context of Einstein's general relativity, dubbed as dark energy (DE) [3–5], or the modification of the gravitational sector of the Universe in various ways [6–15], known as geometrical DE. Apart from DE or geometrical DE, our Universe sector also contains a nonluminous dark matter (DM) fluid responsible for the observed structure formation of the Universe; and according to the high precision data from several astronomical missions, nearly 68% of the total energy density of the Universe is occupied by either DE or geometrical DE, and more or less 28% of the total energy density of the Universe is occupied by DM, that means, nearly 96% of the total energy budget of the Universe is comprised by DE and DM. Thus, the dynamics of the Universe is heavily dependent on the dark sector (DE + DM) of the Universe. However, despite many astronomical missions, the nature, origin, and the evolution of the dark sector have remained mysterious so far, and probing the physics of the dark sector has been one of the challenges for modern cosmology at the present moment. In order to describe the present Universe, several cosmological models have been proposed and investigated by several investigators. Among these models, the Λ-cold dark matter (ΛCDM) cosmological model constructed in the framework of general relativity (GR), in which the cosmological constant Λ plugged into Einstein's gravitational equations acts as the source of DE and DM is cold (pressureless), has been found to be extremely successful in light of a number of observational datasets. Nevertheless, ΛCDM faces several

*sudiphalder197@gmail.com
†jaime.haro@upc.edu
‡tapan.maths@presiuniv.ac.in
§supriya.maths@presiuniv.ac.in

 © 2024 American Physical Society

theoretical and observational challenges, and therefore, a revision of the standard ΛCDM cosmology has been suggested in recent times.

An alternative to the ΛCDM cosmology is the theory of nongravitational interaction between DE and DM, where an energy exchange phenomenon between these dark sectors, widely known as the interacting DE-DM, also known as interacting DE (IDE) or coupled DE cosmology. This particular theory received massive attention in the scientific community for many interesting consequences [16–96] (also see [97–99]), such as, alleviating the cosmic coincidence problem [16,20,100–103], crossing the phantom divide line without invoking any scalar field with negative sign in the kinetic part [104–106], weakening/solving the Hubble constant tension [63,70,75,107–109] between Planck (within ΛCDM paradigm) [110] and SH0ES (supernovae and H_0 for the equation of state of dark energy) [111,112], and the clustering tension [109,113,114] between Planck (within ΛCDM model) and other astronomical probes at low redshifts, e.g., weak gravitational lensing and galaxy clustering [115–124]. In IDE, the dynamics of the dark sector is mainly governed by the choice of a coupling/interacting function Q that controls the transfer of energy between DE and DM, and this coupling function is taken from the phenomenological ground.[1] Now, in the choice of the coupling functions, as they represent the transfer of energy and/or momentum between the DM and DE sectors, Q is usually assumed to be the functions of the energy densities of DE and DM. In general, two varieties of the interaction functions are considered in the literature: (i) the interaction functions where the Hubble rate H of the Friedmann-Lemaître-Robertson-Walker (FLRW) universe explicitly appears, see, for instance, [20–22] and (ii) the interaction functions where H does not appear explicitly, e.g., [29,43,130]. Concerning the above two approaches, even though the interaction between these dark sectors is viewed as a local phenomenon [29], and the presence of the global expansion factor may be avoided, this debate is still unending, and it is very hard to prefer the first approach over the other (see [80]). On the other hand, one can put another question mark on the direction of energy flow between the dark sectors, which is characterized by the choice of the interaction function. In a large class of interaction models, the flow of energy between the dark sectors is assumed to be unidirectional, that means, throughout the period of energy exchange mechanism between the dark sectors, the energy transfer can happen either from "DE to DM" or from "DM to DE." According to the theoretical and observational grounds, there are evidences of the energy transfer from DE to DM [46,70,96], while the direction of energy flow can be reversed in the future [131], but this conclusion depends on the underlying interaction model, properties of DE, and the observational data [92,132],[2] hence, this is one of the interesting questions in the context of interacting DE scenarios. Although these unidirectional interacting scenarios are simple by construction, and they have been widely used in the community, it is very natural to examine whether the direction of energy transfer may alter during the course of energy exchange between the dark sectors. These kinds of interaction models are known as sign changeable or sign shifting interaction functions, and such models are appealing since they allow us to investigate whether the cosmologies with sign changeable interaction models are physically viable. However, because of some unknown reasons, sign changeable interaction models did not get much attention in the community [133–140], but such models are worth investigating in the light of current cosmological tensions [139]. Interestingly, model independent inference on the interaction between the dark sectors as performed in [141] hints for a sign shifting nature of the interaction function. This gives enough motivation to allow a sign changeable nature in the interaction functions and investigate the consequences.

In this article we therefore consider some sign shifting interaction models where the interaction functions depend only on the intrinsic nature of the dark fluids and perform their phase space analysis. As the choice of the interaction functions are not unique, thus, we have considered a variety of interaction functions that have been constructed using the known interaction functions in the literature. On the other hand, as the nature of DE is another unknown character to be discovered (hopefully) with the help of the upcoming astronomical surveys, in this work, in order to be inclusive we have considered that the equation of state of DE could be either constant or dynamical. Now, focusing on the dynamical equation of state of DE, one may have a cluster of possibilities since there is no unique route to determine its expression. Keeping this issue in mind, we have adopted a very well-known dynamical equation of state of DE which depends only on its energy density and having only one free parameter which characterizes the nature of the DE (i.e., where DE is quintessential or phantom) through its sign. This equation of state has been extensively investigated in the cosmological dynamics, and it recovers the usual

[1]Some attempts have been made to derive the coupling functions from an action integral [79,125–129], however, the final destination is yet to be discovered. Thus, at this moment, there is no reason to exclude any possible approach to study the theory of DM-DE interaction, even the approach adopts a phenomenological route.

[2]We note that in Refs. [92,132] the authors have considered various interaction models and constrained them using different datasets, and they reported that both the possibilities, that means the transfer of energy from DE to DM and from DM to DE, are allowed according to the observational datasets. We further mention that the properties of DE (i.e., whether it is quintessence or phantom) and the direction of energy transfer between the dark components are connected with the stability of the interaction model at the level of perturbations, see, for instance, Ref. [83].

barotropic equation of state of DE as a special case. So far as we are aware, the phase space analysis of the proposed sign shifting interacting functions considering both the constant and dynamical equation of state parameters of DE has never been performed in the literature. This is the first time we are reporting the results in the literature.

The article is structured as follows. In Sec. II we introduce the basic equations of an interacting DM-DE model and then propose the models of interaction that we wish to study in this work. In Sec. III we construct the autonomous system corresponding to each interaction function and discuss the nature of the critical points obtained from the interaction functions and also their qualitative behavior in terms of the cosmological parameters. Finally, in Sec. IV we close the article summarizing the key findings.

II. INTERACTING DARK ENERGY

We consider the homogeneous and isotropic universe where its gravitational sector is described by Einstein's GR, and its matter distribution is minimally coupled to gravity. The matter sector consists of two heavy fluids of the Universe, namely, a pressureless (or cold) DM and a DE fluid, which are interacting with each other in a nongravitational way. In order to proceed with the mathematical structure of such scenario, we consider the spatially flat FLRW metric

$$ds^2 = -dt^2 + a^2(t)d\mathbf{x}^2, \tag{1}$$

where t is the comoving time; $a(t)$ is the expansion scale factor of the Universe; $d\mathbf{x}^2$ represents the three-dimensional flat space line element. The Friedmann equations for the above line element can be written as

$$3H^2 = \kappa^2(\rho_c + \rho_d), \tag{2}$$

$$2\dot{H} + 3H^2 = -\kappa^2(p_c + p_d), \tag{3}$$

where an overhead dot denotes the derivative with respect to the cosmic time; $\kappa^2 = 8\pi G$ is Einstein's gravitational constant; $H \equiv \dot{a}(t)/a(t)$ is the Hubble rate of the FLRW universe; ρ_d, p_d are, respectively, the energy density and pressure of the DE fluid obeying the barotropic equation of state $w_d = p_d/\rho_d < -1/3$; ρ_c, p_c are, respectively, the energy density and pressure of DM in the form of dust, i.e., $p_c = 0$, henceforth, we call this DM as cold DM, abbreviated as CDM. As CDM and DE are interacting with each other, therefore, the conservation equations of these dark fluids can be represented as

$$\dot{\rho}_c + 3H\rho_c = -Q(\rho_c, \rho_d), \tag{4}$$

$$\dot{\rho}_d + 3H(1 + w_d)\rho_d = +Q(\rho_c, \rho_d), \tag{5}$$

where $Q(\rho_c, \rho_d)$ denotes the real valued interaction function (also known as the interaction rate) that corresponds to the transfer of energy and (or) momentum between these dark fluids. For $Q(\rho_c, \rho_d) > 0$, energy flow occurs from DM to DE, and for $Q(\rho_c, \rho_d) < 0$, energy flow occurs in the reverse direction, that means from DE to DM. The interaction function $Q(\rho_c, \rho_d)$ is the key ingredient of this scenario because it controls the dynamics of the Universe at the background and perturbation levels. We notice that the conservation equations (4) and (5) can be put in a different format leading to

$$\dot{\rho}_c + 3H(1 + w_{\mathrm{c,eff}})\rho_c = 0, \tag{6}$$

$$\dot{\rho}_d + 3H(1 + w_{\mathrm{d,eff}})\rho_d = 0, \tag{7}$$

which represent a noninteracting scenario of DM and DE with the effective equation of state parameters

$$w_{\mathrm{c,eff}} = \frac{Q(\rho_c, \rho_d)}{3H\rho_c}, \qquad w_{\mathrm{d,eff}} = w_d - \frac{Q(\rho_c, \rho_d)}{3H\rho_d}, \tag{8}$$

from which one can notice that the effective nature of the DM equation of state could be noncold in the sense that the effective equation of state of DM could be nonzero (i.e., $w_{\mathrm{c,eff}} \neq 0$) for $Q(\rho_c, \rho_d) \neq 0$, see, for instance, [142] and, additionally, the effective nature of the DE equation of state could be either quintessential ($w_{\mathrm{d,eff}} > -1$) or phantom ($w_{\mathrm{d,eff}} < -1$) depending on the sign of $Q(\rho_c, \rho_d)$.

Now since the interaction function affects the evolution of both CDM and DE, henceforth, the expansion rate of the universe H will be equally affected and as a result the cosmological parameters will be influenced as well. We introduce the equation of state of the total fluid $w_{\mathrm{tot}} = \frac{\text{total pressure}}{\text{total energy density}} = \frac{p_c + p_d}{\rho_c + \rho_d} = \frac{p_d}{\rho_c + \rho_d}$ (since $p_c = 0$) and the deceleration parameter of the Universe, $q = -(1 + \dot{H}/H^2)$, which take the following forms:

$$w_{\mathrm{tot}} = w_d\Omega_d, \qquad q = \frac{1}{2}(1 + 3w_d\Omega_d), \tag{9}$$

where $\Omega_d = \kappa^2\rho_d/3H^2$ is the density parameter for DE, and from the Friedmann equation (2), one can derive the density parameter for CDM, $\Omega_c (= \kappa^2\rho_c/3H^2)$ as $\Omega_c = 1 - \Omega_d$.

A. Models

In this work we propose several interaction functions having the sign changing property during the evolution of the Universe. One of the important features of all the interaction functions that we are going to propose in this section is that all of them do not depend on the external parameters of the Universe, rather they all depend on the intrinsic nature of the dark sector. The first interaction function in this series has the following form:

$$\text{model I:}\ Q_{\rm I} = \Gamma(\rho_c - \rho_d), \tag{10}$$

where Γ is the coupling parameter of the interaction function measuring the strength of the interaction, and it has the dimension of the Hubble rate H. As argued, Q does not depend on the external parameters of the Universe, e.g., the scale factor of the Universe or its expansion rate, rather it depends on the intrinsic properties of DM and DE, namely, their energy densities, ρ_c and ρ_d. Hence, one may expect that this interaction model could offer some inherent nature of the dark components. We further note that $Q_{\rm I}$ may change its sign depending on the dominating role played by one of the fluids, that means, if the dominating role played by DM over DE ($\rho_c > \rho_d$) is suddenly altered, i.e., DE starts dominating over DM as in the late time accelerating phase ($\rho_d > \rho_c$), then $Q_{\rm I}$ shifts its sign.

We generalize the sign-shifting interaction function of Eq. (10) as follows:

$$\text{model II:}\ Q_{\rm II} = \Gamma_c\rho_c - \Gamma_d\rho_d, \tag{11}$$

where Γ_c and Γ_d are the coupling parameters of the interaction function having the dimension equal to the dimension of the Hubble parameter. For the interaction function $Q_{\rm II}$ to be sign changeable, both the coupling parameters Γ_c, Γ_d should have the same sign, that means either $\Gamma_c > 0$, $\Gamma_d > 0$ or $\Gamma_c < 0$, $\Gamma_d < 0$, but never $\Gamma_c\Gamma_d < 0$. Similar to the earlier interaction function, this model also does not include any external parameters of the Universe.

The next model in this series that we introduce has the following form:

$$\text{model III:}\ Q_{\rm III} = \Gamma\left(\rho_c - \rho_d - \frac{\rho_c\rho_d}{\rho_c + \rho_d}\right), \tag{12}$$

where as already noted, Γ is the coupling parameter of the interaction function having the dimension equal to the dimension of the Hubble parameter. Notice that the interaction function (12) is obtained by including a new function $Q_{\rm new} = -\Gamma\rho_c\rho_d(\rho_c + \rho_d)^{-1}$ with the model of Eq. (10), that means $Q_{\rm III} = Q_{\rm I} + Q_{\rm new}$. Similar to the earlier two interaction functions, here too, we notice that this interaction function depends only on the intrinsic nature of the dark fluids.

Lastly, we introduce two new interactions of the forms

$$\text{model IV:}\ Q_{\rm IV} = \Gamma_c\rho_c - \Gamma_{cd}\frac{\rho_c\rho_d}{\rho_c + \rho_d}, \tag{13}$$

and

$$\text{model V:}\ Q_{\rm V} = \Gamma_d\rho_d - \Gamma_{cd}\frac{\rho_c\rho_d}{\rho_c + \rho_d}, \tag{14}$$

where Γ_c, Γ_d, and Γ_{cd} are the coupling parameters, and they all have the dimension of the Hubble parameter. One can easily notice that the last term of both model IV [Eq. (13)] and model V [Eq. (14)] are the same but the models differ in their first terms containing ρ_c and ρ_d, respectively. We further note that Γ_c, Γ_d, and Γ_{cd} are all constants in such a way so that the models allow sign shifting property. That means, for model IV [Eq. (13)], Γ_c and Γ_{cd} will enjoy the same sign, and for model V [Eq. (14)], Γ_d and Γ_{cd} will enjoy the same sign, but $\Gamma_c \neq \Gamma_{cd}$ for model IV, and $\Gamma_d \neq \Gamma_{cd}$ for model V, otherwise $Q_{\rm IV}$ and $Q_{\rm V}$ will represent the energy flow only in one direction. The choice of the interaction function is not unique, therefore, one can construct a variety of such models, however, it should be kept in mind that the interaction functions may lead to negative energy densities of the dark sectors as argued in [130], hence, working with an arbitrary interaction function needs precaution.

III. DYNAMICAL ANALYSIS OF INTERACTING MODELS

The dynamical analysis of the interaction models is the heart of this work. The dynamical analysis plays a crucial role in understanding the local and global dynamics of the underlying cosmological scenarios. In order to perform the dynamical analysis of the underlying interacting scenarios, one needs to define a new set of dimensionless variables in terms of which one can study the behavior of the system of differential equations. We refer to [27,143–165] (also see the review article [166] and the references therein) where several interacting scenarios have been studied through the dynamical system analysis. In this section we shall describe the dynamical systems for the proposed sign-shifting interaction models. Additionally, we shall also show that the choice of the dimensionless variables is extremely important because for a wrong choice of these variables, one may not be able explore the whole space of critical points.

A. Model I

We begin our analysis with the first interaction function $Q_{\rm I}$ of Eq. (10), and we define the following dimensionless variables:

$$x = \frac{\kappa^2\rho_c}{3H^2}, \qquad y = \frac{H_0}{H}, \tag{15}$$

where H_0 (> 0) is a constant, and here it denotes the present value of the Hubble parameter.[3] The density parameters for CDM, DE, the equation state of the total fluid, $w_{\rm tot}$, and the deceleration parameter q can be expressed in terms of the dimensionless parameters as follows:

[3]Note that instead of taking H_0, one may consider any $\tilde{H}$ which is also constant so that $y = \tilde{H}/H$ becomes dimensionless.

$$\Omega_c = x, \qquad \Omega_d = 1 - x,$$
$$w_{\rm tot} = w_d(1-x), \qquad q = \frac{1}{2}[1 + 3w_d(1-x)].$$

Now, inserting the dimensionless variables of Eq. (15) into the equations of motion (2)–(4), and using the interaction function $Q_{\rm I}$ of Eq. (10), we have the following autonomous system:

$$x' = -\gamma y(2x-1) + 3w_d x(1-x), \tag{16}$$

$$y' = \frac{3}{2}y(1 + w_d(1-x)), \tag{17}$$

where a prime over a variable denotes its differentiation with respect to $N = \ln(a/a_0)$ (here a_0 is the present value of the scale factor), and γ is defined as $\gamma = \Gamma/H_0$, hence, γ becomes a dimensionless parameter. The critical points of the autonomous system (16) and (17) are obtained by solving the equations $x' = 0$ and $y' = 0$. In this case we have three critical points $A_1 = (0,0)$, $A_2 = (1,0)$, and $A_3 = (\frac{1+w_d}{w_d}, -\frac{3(1+w_d)}{\gamma(2+w_d)})$.

In order to better understand the dynamical system when the Hubble rate is small, it will be useful to use the variables (x, H). Now, using the cosmic time derivative, the dynamical system for the variables (x, H) becomes

$$\begin{cases} \dot{x} = -\Gamma(2x-1) + 3w_d H x(1-x), \\ \dot{H} = -\frac{3}{2}H^2(1 + w_d(1-x)). \end{cases} \tag{18}$$

On can see that the autonomous system (18) has only two critical points, namely, $A_0 = (\frac{1}{2}, 0)$ and $(\frac{1+w_d}{w_d}, -\frac{\Gamma(2+w_d)}{3(1+w_d)})$, which is actually A_3 if we consider this critical point in terms of (x, y) coordinates. Here, it is important to understand that the point A_0 does not appear in the coordinates (x, y) because it corresponds to $y = \infty$, and for the same reason the points A_1 and A_2 do not appear in the coordinates (x, H) because they correspond to $H = \infty$. This clearly indicates that the above two autonomous systems are not giving the complete information.

For this reason it is important to get a new coordinate system where all the critical points appear. This could be done by introducing a new variable,

$$z = \frac{y}{1+y} = \frac{H_0}{H + H_0}, \tag{19}$$

where $H = 0$ corresponds to $z = 1$, and $H = \infty$ corresponds to $z = 0$. So, in the new coordinates (x, z) the dynamical system (16) and (17) becomes

$$\begin{cases} x' = -\gamma\left(\frac{z}{1-z}\right)(2x-1) + 3w_d x(1-x), \\ z' = \frac{3}{2}(1-z)z(1 + w_d(1-x)). \end{cases} \tag{20}$$

But, note that, the dynamical system (20) is singular at $z = 1$ (i.e., $H = 0$). Thus, in order to regularize it, and taking into account that the phase portrait does not change topologically when one multiplies the vector field by a positive function, we regularize it by multiplying the factor $(1 - z)$, which leads to the regular dynamical system

$$\begin{cases} x' = -\gamma z(2x-1) + 3(1-z)w_d x(1-x), \\ z' = \frac{3}{2}(1-z)^2 z(1 + w_d(1-x)). \end{cases} \tag{21}$$

Thus, finally one can investigate the dynamical system (21) through the stability analysis of the critical points. The physical domain, namely R, is the square $R = [0,1]^2$, which in order to be positively invariant, i.e., to ensure that a solution of the dynamical system with initial conditions in R never leaves it, one has to impose that $\gamma > 0$ (i.e., $\Gamma > 0$). Effectively, it follows from Eq. (20) that close to $x = 0$, one has $x' \cong \gamma z > 0$ and close to $x = 1$, one has $x' \cong -\gamma z < 0$. For $z = 0$ and $z = 1$, one has $z' = 0$, meaning that, for $\gamma > 0$, the dynamical system never crosses the lines $x = 0$, $x = 1$, $z = 0$, and $z = 1$, that is, the domain R is positively invariant. As the dynamical system contains the DE equation of state, which could be either constant or dynamical, therefore, we aim to investigate both the cases separately. In the following we present our analyses for constant w_d and dynamical w_d.

1. Constant w_d

Considering that the DE equation of state w_d is constant, in Table I we present the critical points of the dynamical system (21), their existence, stability, and the values of the cosmological parameters evaluated at those critical points. Now depending on the nature of w_d, it is comprehensible

TABLE I. The critical points, their existence, stability, and the values of the cosmological parameters evaluated at those points for the interacting scenario driven by the interaction function $Q_{\rm I} = \Gamma(\rho_c - \rho_d)$ of Eq. (10) are summarized.

Point	x	z	Existence	Stability	Acceleration	Ω_c	Ω_d	$w_{\rm tot}$
A_0	$\frac{1}{2}$	1	For all $\gamma > 0$ and $w_d < -1/3$	Stable for $-2 < w_d < -1/3$	$w_d < -2/3$	1/2	1/2	$w_d/2$
A_1	0	0	For all $\gamma > 0$ and $w_d < -\frac{1}{3}$	Stable for $w_d < -1$	$w_d < -\frac{1}{3}$	0	1	w_d
A_2	1	0	For all $\gamma > 0$ and $w_d < -\frac{1}{3}$	Unstable	No	1	0	0
A_3	$\frac{1+w_d}{w_d}$	$-\frac{3(1+w_d)}{2\gamma-3+w_d(\gamma-3)}$	For all $\gamma > 0$ and $-2 \le w_d \le -1$	Unstable	Yes	$\frac{1+w_d}{w_d}$	$-\frac{1}{w_d}$	-1

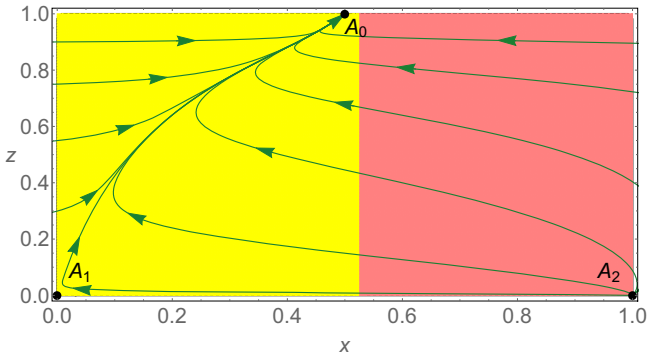

FIG. 1. The phase portrait plot describing model I [Eq. (10)] with $w_d \geq -1$ and $\gamma > 0$. In this case we have taken $w_d = -0.95$ and $\gamma = 0.4$. We note that one can take any value of $w_d \geq -1$ and any positive value of γ in order to get similar graphics. Here, the yellow shaded region represents the accelerated region (i.e., $q < 0$), and the pink shaded region corresponds to the decelerated region (i.e., $q > 0$).

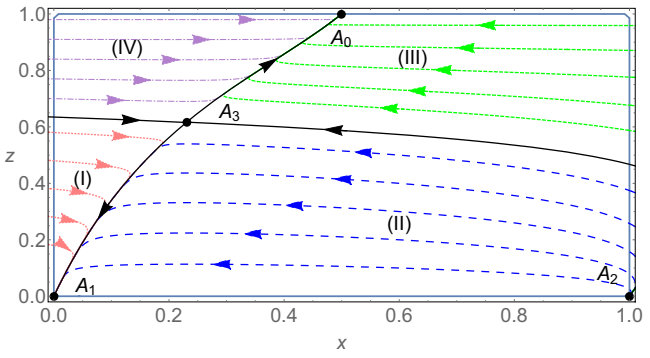

FIG. 2. The phase portrait plot describing model I [Eq. (10)] for $-2 < w_d < -1$ and $\gamma > 0$. In this case we have taken $w_d = -1.3$ and $\gamma = 0.8$. We note that one can take any specific value of $\gamma(> 0)$ to draw the plot, however, as long as γ decreases, regions I and IV become very small, and they look indistinguishable from one another.

that the nature of the critical points will certainly be affected. Thus, in order to be precise, we divide the entire parameter space of w_d into three disjoint regions, namely, quintessence or nonphantom ($w_d > -1$), cosmological constant ($w_d = -1$), and phantom ($w_d < -1$). In the following we present how w_d affects the nature of the critical points.

(1) For nonphantom dark energy, i.e., when $w_d > -1$, the point A_3 does not belong to the physical domain R. In addition, since $w_{\rm tot} = w_d(1-x)$, this means that $w_{\rm tot} > -1$, and taking into account that $z' = \frac{3}{2}(1-z)^2 z(1+w_d(1-x))$, we have $z' > 0$. So, A_1 and A_2 are unstable. On the line $z = 1$, we have $z' = 0$, $x' < 0$ for $x > 1/2$ and $x' > 0$ for $x < 1/2$. Thus, the critical point A_0 is stable, in fact, it is a global attractor. Therefore, at late times, the Universe accelerates with $w_{\rm tot} = w_d/2 > -1$, when $-1 < w_d < -2/3$, and it decelerates when $-2/3 < w_d < -1/3$. In addition, since $w_{\rm tot} > -1$ the Hubble rate decreases to zero, and $\Omega_d = \Omega_c = 1/2$. The phase plot is shown in Fig. 1. This finishes the study for a nonphantom dark energy.

(2) When $w_d = -1$, one has $A_1 = A_3$. In this case, the linearization does not decide the nature of the critical point A_1. In fact, A_1 and A_2 are unstable because $z' = \frac{3}{2}(1-z)^2 zx > 0$, for $0 < z < 1$ and $x > 0$. Moreover, only the unphysical orbit $z = 0$ ($H = \infty$) converges to A_1. Now, on $z = 1$ line, we obtain $z' = 0$, $x' < 0$ for $x > 1/2$ and $x' > 0$ for $x < 1/2$. Consequently, in this case A_0 is a global attractor. Again, the phase plot is given in Fig. 1.

(3) For a phantom dark fluid, two cases arise:

(a) When $-2 < w_d < -1$: The critical point A_3 belongs to the physical region R. Clearly, we obtain $0 < (1+w_d)/w_d < 1/2$. Whenever $x < (1+w_d)/w_d$, we get $1 + w_{\rm tot} < 0$, and so, z' is negative. Similarly, we have $1 + w_{\rm tot} > 0$ for $x > (1+w_d)/w_d$ and as a result z' is positive. On $z = 1$ line, we obtain $z' = 0$, $x' < 0$ for $x > 1/2$ and $x' > 0$ for $x < 1/2$. Again, on $z = 0$ line, $z' = 0$ and $x' = 3w_d x(1-x)$, which is negative. Therefore, our domain R is divided into four regions. Thus, an orbit in regions I and II of Fig. 2, at late times, converges to A_1. For an orbit in regions III and IV, at late time, it converges to A_0. Note that A_0 means $H = 0$ with $\Omega_c = \Omega_d = 1/2$ and $w_{\rm tot} = w_d/2 > -1$. On the contrary, A_1 means $H = \infty$ with $\Omega_d = 1$ and $w_{\rm tot} = w_d < -1$. Figure 3 shows the evolution of the density parameters, namely, Ω_c, Ω_d, and the total equation of state parameter, $w_{\rm tot}$.

(b) When $w_d \leq -2$: For the particular case with $w_d = -2$, which represents a very high phantom regime, $A_3 = A_0$. Here, $(1+w_d)/w_d = 1/2$, so we have $z' < 0$ for $x < 1/2$ and $z' > 0$ for $x > 1/2$. On the line $z = 0$, we obtain $z' = 0$ and $x' < 0$. Therefore, A_0, A_2 are unstable, and A_1 becomes a global attractor. When $-2 > w_d$, the critical point A_3 does not belong to the physical region R. Again, $(1+w_d)/w_d > 1/2$, which implies that $z' < 0$ if $x < (1+w_d)/w_d$, and $z' > 0$ if $x > (1+w_d)/w_d$. Thus, A_0, A_2 are unstable, and A_1 is a global attractor. Figure 4 exhibits the behavior.

2. Dynamical w_d

The case with dynamical equation of state of DE w_d is interesting for two reasons. First of all, the autonomous system (21) with constant w_d is a special case of the

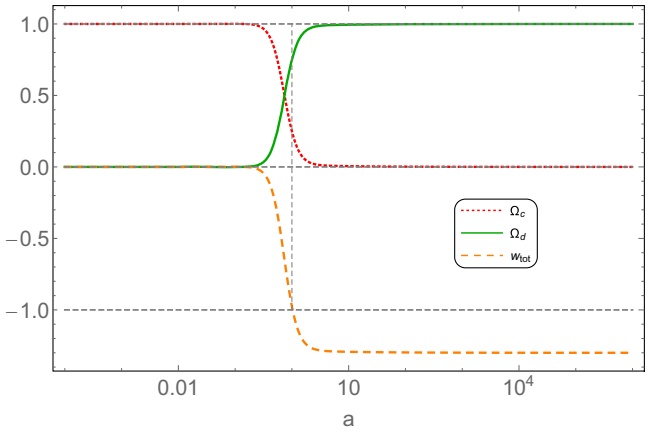

FIG. 3. We show the evolution of the CDM density parameter (Ω_c), dark energy density parameter (Ω_d), and the total equation of state (EOS) parameter ($w_{\rm tot}$) for model I [Eq. (10)] for $-2 < w_d < -1$. We have taken $w_d = -1.3$, $\gamma = 0.8$ with the initial conditions $x(N=0) = 0.25$, $z(N=0) = 0.05$ taken from region II of Fig. 2. For the initial condition on $x(N)$ and $z(N)$ from region I of Fig. 2, again we shall obtain $\Omega_c = 0$ and $\Omega_d = 1$ at late time. If we choose the initial conditions on $x(N)$ and $y(N)$ from regions III and IV of Fig. 2, we shall reach $\Omega_c = \Omega_d = 1/2$ in an asymptotic way.

dynamical w_d case. On the other hand, and most importantly, the dynamical w_d scenario may offer a bigger space of critical points, and hence one may expect new results in this context. In this article, we shall consider a parametric form for w_d to investigate the autonomous system (21). The choice of the dynamical w_d is not unique, and one can consider a variety of choices. The question then arises, what should be a possible choice for w_d to proceed with the analysis? A possible choice for dynamical w_d capturing a wide variety of models in this direction may take the following form [167,168]:

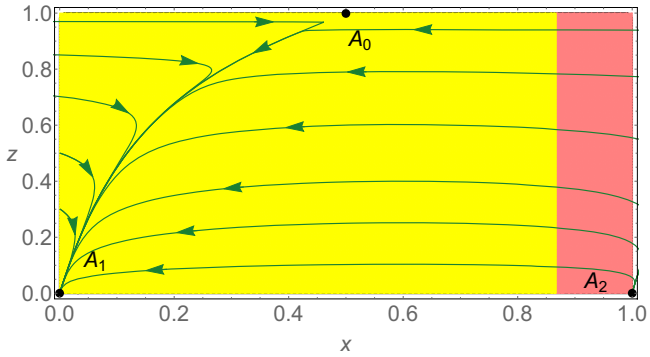

FIG. 4. The phase portrait plot describing model I of (10) with $w_d \leq -2$ and $\gamma > 0$. In this case we have taken $w_d = -2.5$ and $\gamma = 0.8$. We note that one can take any value of $w_d \leq -2$ and any positive value of γ in order to get similar graphics. Here, the yellow shaded region represents the accelerated region (i.e., $q < 0$), and the pink shaded region corresponds to the decelerated region (i.e., $q > 0$).

$$p_d = -\rho_d - f(\rho_d), \tag{22}$$

where f is any analytic function of ρ_d. Notice from (22) that $w_d = p_d/\rho_d = -1 - f(\rho_d)/\rho_d$ describes a deviation from the cosmological constant $w_d = -1$ through the dynamical term $f(\rho_d)/\rho_d$. A general choice of this equation of state could be $p_d = -\rho_d - A\rho_d^n$, where n and A are constants in which n is a dimensionless constant, but A has dimension. We restrict ourselves to $n = 2$ in this article for which we have

$$p_d = -\rho_d - A\rho_d^2 \Leftrightarrow w_d = -1 - A\rho_d. \tag{23}$$

Now, for the equation of state (23), the autonomous system (20) becomes

$$\begin{cases} x' = -\gamma\left(\frac{z}{1-z}\right)(2x-1) - 3x(1-x)\left(1+\nu\frac{(1-z)^2(1-x)}{z^2}\right), \\ z' = \frac{3}{2}(1-z)z\left(x - \nu\frac{(1-z)^2(1-x)^2}{z^2}\right), \end{cases} \tag{24}$$

where $\nu = \frac{3AH_0^2}{\kappa^2}$. We regularize the autonomous system (24) by multiplying the factor $z^2(1-z)$ on the right hand sides of (24) and finally obtain

$$\begin{cases} x' = -\gamma z^3(2x-1) - 3(1-z)x(1-x)(z^2 + \nu(1-z)^2(1-x)), \\ z' = \frac{3}{2}(1-z)^2 z(xz^2 - \nu(1-z)^2(1-x)^2). \end{cases} \tag{25}$$

Note that the qualitative behavior for both the autonomous systems (24) and (25) remain topologically equivalent. From the autonomous system (25), one can now find the critical points by solving the equations $x' = 0$ and $z' = 0$, and the critical points of the system (25) are

$$\bar{A}_0 = \left(\frac{1}{2}, 1\right), \qquad \bar{A}_1 = (0,0), \qquad \bar{A}_2 = (1,0),$$
$$S = \left\{\left(x_c, \frac{3x_c}{3x_c - \gamma(2x_c - 1)}\right)\right\},$$

where S is the set of critical points in which x_c denotes a real root of $f(x) \equiv 9x^3 - \nu\gamma^2(2x-1)^2(1-x)^2 = 0$.[4] Since, $f(x)$ is a fourth degree equation in x, the set S may contain a maximum of four critical points.

Now, as the physical domain in our case is $R = [0,1]^2$, therefore, we are interested in investigating the number of roots of $f(x)$ in [0, 1]. As $f(0) = -\gamma^2\nu < 0$ (for $\nu > 0$) and

[4]We note that $f(x)$ can be obtained from the following two nullclines:

$$xz^2 - \nu(1-z)^2(1-x)^2 = 0, \tag{26}$$

$$-\gamma z^3(2x-1) - 3x(1-x)(1-z)[z^2 + \nu(1-z)^2(1-x)] = 0. \tag{27}$$

TABLE II. The critical points, their existence, stability, and the values of the cosmological parameters evaluated at those points for the interacting scenario driven by the interaction function $Q_{\rm II} = \Gamma_c\rho_c - \Gamma_d\rho_d$ of Eq. (11) are summarized.

Point	x	z	Existence	Stability	Acceleration	Ω_c	Ω_d	$w_{\rm tot}$
B_0	$\frac{\beta}{\alpha+\beta}$	1	$\alpha(>0), \beta(>0)$ and $w_d < -\frac{1}{3}$	$-1-\frac{\beta}{\alpha} < w_d < -\frac{1}{3}$	$w_d < -\frac{1}{3}(1+\frac{\beta}{\alpha})$	$\frac{\beta}{\alpha+\beta}$	$\frac{\alpha}{\alpha+\beta}$	$\frac{\alpha w_d}{\alpha+\beta}$
B_1	0	0	$\alpha(>0), \beta(>0)$ and $w_d < -\frac{1}{3}$	$w_d < -1$	$w_d < -\frac{1}{3}$	0	1	w_d
B_2	1	0	$\alpha(>0), \beta(>0)$ and $w_d < -\frac{1}{3}$	Unstable	No	1	0	0
B_3	$\frac{1+w_d}{w_d}$	$-\frac{3(1+w_d)}{(\alpha-3)w_d+(\alpha+\beta-3)}$	$\alpha(>0), \beta(>0)$ and $-1-\frac{\beta}{\alpha} \le w_d \le -1$	Unstable	Yes	$\frac{1+w_d}{w_d}$	$-\frac{1}{w_d}$	-1

$f(1) = 9 > 0$, hence, by the Bolzano's theorem[5] [169], $f(x)$ will have at least one real root in (0, 1). Here we argue that f will have only one real root in (0, 1). It also follows that since $0 < x_c < 1$, therefore, the condition $z = \frac{3x_c}{3x_c-\gamma(2x_c-1)} \le 1$ leads to $x_c \le 1/2$. Hence, our domain is slightly reduced, and we need to check the number of roots of $f(x)$ in $[0, 1/2]$. Since we have $f(1/2) = 9/8 > 0$, it follows from the Bolzano's theorem [169] that there is at least one real root of $f(x)$ in $(0, 1/2)$. Now, looking at the derivative of $f(x)$ with respect to x, given by $f'(x) = -16\gamma^2\nu(x-1)(x-\frac{3}{4})(x-\frac{1}{2}) + 27x^2$, one can check that $f'(x) > 0$ for all $x \in (0, 1/2)$. This shows that the function $f(x)$ is strictly increasing in $(0, 1/2)$, and consequently, $f(x)$ has only one root in $(0, 1/2)$. This concludes that the set S has only one critical point in the physical domain R, and we label this critical point as $\bar{A}_3$. Now, in this case, we observe that the point $\bar{A}_3$ behaves qualitatively the same as the point A_3 described earlier, and correspondingly, the phase portrait is the same as Fig. 2.

On the other hand, for $\nu < 0$, the algebraic curve represented by the Eq. (26) has no branches in the positive quadrant. Hence, for $\nu < 0$, S is an empty set, and as a result, the autonomous system for $\nu < 0$ admits only three critical points, namely, $\bar{A}_0$, $\bar{A}_1$, $\bar{A}_2$. The corresponding phase plot will be similar to Fig. 1.

B. Model II

We now consider the second interaction model in this series, i.e., $Q_{\rm II}$ of (11). Notice that $Q_{\rm II}$ has two coupling parameters Γ_c and Γ_d. As demonstrated in Sec. III A, here we shall consider the following dimensionless variables

$$x = \frac{\kappa^2\rho_c}{3H^2}, \qquad z = \frac{H_0}{H+H_0}, \tag{28}$$

in order to understand the dynamics of the interacting scenario. With these choices of the dynamical variables, the autonomous system for this interaction function can be expressed as

$$\begin{cases} x' = -\frac{z}{1-z}[\alpha x - \beta(1-x)] + 3w_d x(1-x), \\ z' = \frac{3}{2}(1-z)z(1+w_d(1-x)), \end{cases} \tag{29}$$

where α, β are the dimensionless parameters defined as $\alpha = \Gamma_c/H_0$, $\beta = \Gamma_d/H_0$. Now, regularizing (29) we get

$$\begin{cases} x' = -z[\alpha x - \beta(1-x)] + 3(1-z)w_d x(1-x), \\ z' = \frac{3}{2}(1-z)^2 z(1+w_d(1-x)). \end{cases} \tag{30}$$

The physical domain, namely R, is the square $R = [0, 1]^2$, and it follows from the autonomous system (30) that along the lines $x = 0$ and $x = 1$, one has $x' = \beta z$ and $x' = -\alpha z$, and also the lines $z = 0$ and $z = 1$ remain invariant. Thus, to ensure that the physical domain R is positively invariant we have to restrict our attention on $\alpha > 0$ and $\beta > 0$ (i.e., $\Gamma_c > 0$ and $\Gamma_d > 0$), and therefore, $Q_{\rm II}$ may allow a sign change during the evolution of the Universe without exhibiting any unphysical properties in the energy densities of the dark sector.

Now, in a similar fashion we focus on two cases, namely, the constant w_d and dynamical w_d. In the following we consider both the possibilities.

1. Constant w_d

Considering w_d as a constant, in Table II we summarize the critical points of the autonomous system (30), their existence and stability, as well as the cosmological parameters evaluated at those critical points. Now we consider three different regions of w_d as follows: if w_d has a quintessential nature (i.e., $w_d > -1$), if w_d mimics a cosmological constant (i.e., $w_d = -1$), and if w_d has a phantom character ($w_d < -1$). In what follows we investigate each case.

(1) When $w_d > -1$, the point B_3 does not belong to the physical domain R. Now, we can see that on $z = 1$ line, we have $z' = 0$, $x' > 0$ for $x < \frac{\beta}{\alpha+\beta}$ and $x' < 0$ for $x > \frac{\beta}{\alpha+\beta}$. Also, we have $w_{\rm tot} = w_d(1-x) > -1$, which implies $z' = \frac{3}{2}z(1-z)^2(1+w_{\rm tot}) > 0$. So, B_1, B_2 are unstable critical points, and B_0 is a

[5]Bolzano's theorem: Let f be a real valued and continuous function in a compact interval $[k, l]$ in $\mathbb{R}$ and suppose that $f(k)$, $f(l)$ have opposite signs, that means $f(k)f(l) < 0$. Then there is at least one point m in (k, l) such that $f(m) = 0$.

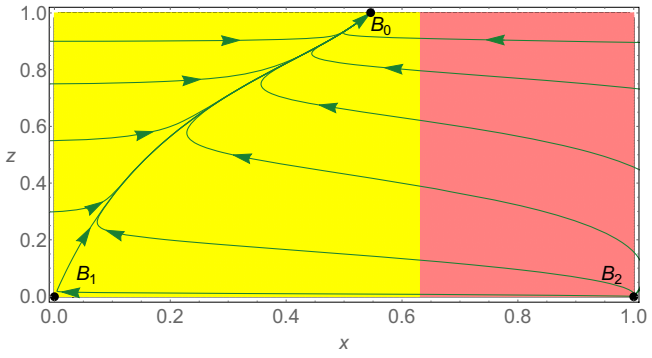

FIG. 5. Phase portrait plot depicting model II [Eq. (11)] with $\alpha > 0$, $\beta > 0$ and $w_d \geq -1$. In this case we have taken $w_d = -0.9$, $\alpha = 0.5$, and $\beta = 0.6$. We note that one can take any value of $w_d \geq -1$ and any positive value of α and β in order to get similar graphics. Here, the yellow shaded region represents the accelerated region (i.e., $q < 0$), and the pink shaded region corresponds to the decelerated region (i.e., $q > 0$).

global attractor. Note that B_0 corresponds to $H = 0$, $\Omega_c = \frac{\beta}{\alpha+\beta}$, and $\Omega_d = \frac{\alpha}{\alpha+\beta}$. The qualitative behavior is displayed in Fig. 5.

(2) When $w_d = -1$, we have $B_3 = B_1$. Again, in this case, on the line $z = 1$, one has $z' = 0$, $x' > 0$ for $x < \frac{\beta}{\alpha+\beta}$ and $x' < 0$ for $x > \frac{\beta}{\alpha+\beta}$. Noting that $z' = \frac{3}{2}z(1-z)^2 x$ is positive. Thus, B_1, B_2 are unstable, and B_0 is a global attractor. Again, Fig. 5 shows the phase plot.

(3) Now dealing with a phantom dark energy fluid, we have the following results:

(a) When $-1 - \frac{\beta}{\alpha} < w_d < -1$, the point B_3 belongs to the physical domain, and we get $0 < \frac{1+w_d}{w_d} < \frac{\beta}{\alpha+\beta}$. Also, we have $z' < 0$ for $x < \frac{1+w_d}{w_d}$ and $z' > 0$ for $x > \frac{1+w_d}{w_d}$. On $z = 0$ line, x' is negative. Again, on the line $z = 1$, x' is positive for $x < \frac{\beta}{\alpha+\beta}$, and x' is negative for $x > \frac{\beta}{\alpha+\beta}$. Thus, we have two "invariant stable orbits" (see Fig. 6) which divide the physical domain into two parts. The orbits below these "invariant manifolds" converge to B_1, and the orbits above them converge to B_0. Figure 7 displays the evolution of the density parameters, namely, Ω_c, Ω_d, and the total equation of state parameter $w_{\rm tot}$.

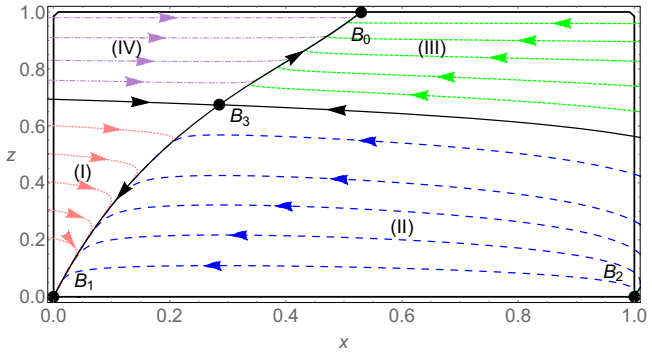

FIG. 6. Phase plot for model II [Eq. (11)] with $\alpha > 0, \beta > 0$ and $-1 - \frac{\beta}{\alpha} < w_d < -1$. Here, we have taken $w_d = -1.4$, $\alpha = 0.8$, and $\beta = 0.9$. Note that one can take any specific value of $\alpha(> 0)$ and $\beta(> 0)$ to draw the plot, however, as long as α and β decrease, regions I and IV become very small, and they look indistinguishable from one another.

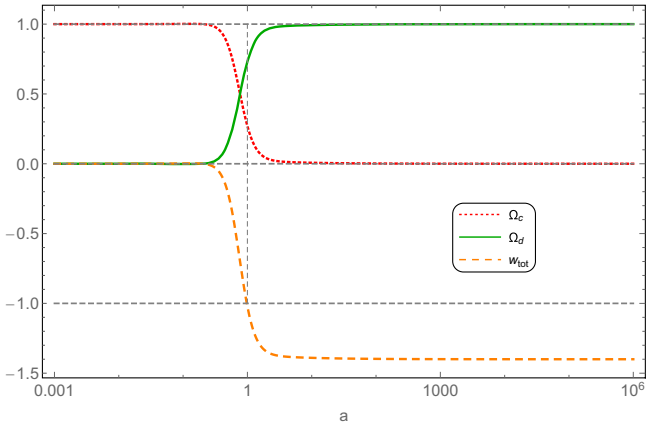

FIG. 7. We show the evolution of the CDM density parameter (Ω_c), dark energy density parameter (Ω_d), and the total EOS parameter ($w_{\rm tot}$) for model II [Eq. (11)]. We have taken the following values of the parameters: $w_d = -1.4$, $\alpha = 0.8$, $\beta = 0.9$ and the following initial conditions $x(N = 0) = 0.27$, $z(N = 0) = 0.08$ from region II of Fig. 6. For the values of initial conditions on $x(N)$ and $y(N)$ from region I, in a similar fashion, we shall obtain $\Omega_c = 0$ and $\Omega_d = 1$ at late time. Again if we take initial conditions on $x(N)$ and $y(N)$ from regions III and IV of Fig. 6, we shall reach $\Omega_c = \frac{\beta}{\alpha+\beta}$ and $\Omega_d = \frac{\alpha}{\alpha+\beta}$ in an asymptotic fashion.

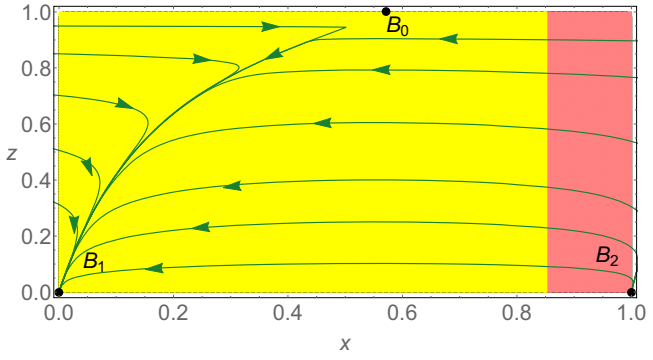

FIG. 8. Phase portrait plot for model II [Eq. (11)] with $\alpha > 0$, $\beta > 0$ and $w_d \leq -1 - \frac{\beta}{\alpha}$. In this case we have taken $w_d = -2.4$, $\alpha = 0.6$, and $\beta = 0.8$. We note that one can take any value of $w_d \leq -1 - \frac{\beta}{\alpha}$ and any positive value of α and β in order to get similar graphics. Here, the yellow shaded region represents the accelerated region (i.e., $q < 0$), and the pink shaded region corresponds to the decelerated region (i.e., $q > 0$).

(b) When $w_d = -1 - \frac{\beta}{\alpha}$, we have $B_0 = B_3$ and $\frac{1+w_d}{w_d} = \frac{\beta}{\alpha+\beta}$. For $x < \frac{1+w_d}{w_d}$, one has $z' < 0$ and for $x > \frac{1+w_d}{w_d}$, z' is positive. Since $x' < 0$ on $z = 0$, B_1 is a global attractor. The qualitative behavior is given in Fig. 8.

(c) When $w_d < -1 - \frac{\beta}{\alpha}$, the point B_3 does not belong to the physical domain R. Here, we obtain $\frac{1+w_d}{w_d} > \frac{\beta}{\alpha+\beta}$, $z' < 0$ if $x < \frac{1+w_d}{w_d}$ and $z' > 0$ if $x > \frac{1+w_d}{w_d}$. On $z = 0$ line, we have $x' = 3w_d x(1-x)$, which is negative. Therefore, B_0, B_1 are unstable critical points, and once again B_1 is a global attractor. Figure 8 exhibits the nature of phase portrait.

2. Dynamical w_d

Now, consider the dynamical w_d as in Eq. (23), for which the autonomous system (29) takes the form

$$\begin{cases} x' = -\left(\frac{z}{1-z}\right)(\alpha x - \beta(1-x)) - 3x(1-x)\left(1 + \nu\frac{(1-z)^2(1-x)}{z^2}\right), \\ z' = \frac{3}{2}(1-z)z\left(x - \nu\frac{(1-z)^2(1-x)^2}{z^2}\right), \end{cases} \tag{31}$$

where $\nu = \frac{3AH_0^2}{\kappa^2}$. We regularize the autonomous system (31) by multiplying the factor $z^2(1-z)$ on the right hand sides of (31) and finally obtain the following autonomous system, which is topologically equivalent to (31):

$$\begin{cases} x' = -z^3(\alpha x - \beta(1-x)) - 3(1-z)x(1-x)(z^2 + \nu(1-z)^2(1-x)), \\ z' = \frac{3}{2}(1-z)^2 z(xz^2 - \nu(1-z)^2(1-x)^2). \end{cases} \tag{32}$$

Now, the critical points of the system (32) are

$$\bar{B}_0 = \left(\frac{\beta}{\alpha+\beta}, 1\right), \qquad \bar{B}_1 = (0,0),$$
$$\bar{B}_2 = (1,0), \qquad S = \left\{\left(x_c, \frac{3x_c}{3x_c - (\alpha+\beta)x + \beta}\right)\right\},$$

where S represents the set of critical points in which x_c denotes a real root of $h(x) \equiv 9x^3 - \nu((\alpha+\beta)x - \beta)^2 \times (1-x)^2 = 0$.[6] As $h(x)$ is a fourth degree equation in x, therefore, the set S may contain a maximum of four critical points. Now, since our physical domain is R, therefore, we are interested in investigating the number of roots of $h(x)$ within the interval [0, 1]. As $h(0) = -\beta^2\nu < 0$ (for $\nu > 0$) and $h(1) = 9 > 0$, hence, by the Bolzano's theorem [169], $h(x)$ will have at least one real root in (0, 1). Note that the z component of the critical point should satisfy $0 \le z \le 1$. Now, for any x_c in (0, 1), the condition on the z component, $\frac{3x_c}{3x_c-(\alpha+\beta)x+\beta} \le 1$ leads to $x_c \le \beta/(\alpha+\beta)$. Consequently, we need to check the number of roots of $h(x)$ in $[0, \frac{\beta}{\alpha+\beta}]$.

[6]Note that $h(x)$ can be obtained from the following two nullclines:

$$xz^2 - \nu(1-z)^2(1-x)^2 = 0, \tag{33}$$

$$-z^3[\alpha x - \beta(1-x)] - 3x(1-x)(1-z)[z^2 + \nu(1-z)^2(1-x)] = 0. \tag{34}$$

Again, we notice that $h(0) < 0$ and $h(\beta/(\alpha+\beta)) = 9((\beta/(\alpha+\beta))^3 > 0$ (since $\alpha > 0$, $\beta > 0$). Thus, from the Bolzano's theorem [169], we claim that there is at least one root of $h(x)$ in $(0, \beta/(\alpha+\beta))$. Now, looking at the derivative of $h(x)$ given by

$$h'(x) = -4(\alpha+\beta)^2\nu(x-1)\left(x - \frac{\beta}{\alpha+\beta}\right)\left(x - \frac{\alpha+2\beta}{2\alpha+2\beta}\right) + 27x^2,$$

we can see that $h'(x)$ is positive in $(0, \beta/(\alpha+\beta))$ i.e., $h(x)$ is strictly increasing in $(0, \beta/(\alpha+\beta))$. Hence, $h(x)$ has only one root in $(0, \beta/(\alpha+\beta))$, and correspondingly, the set S contains only one critical point, and we label this critical point as $\bar{B}_3$. In this case, we also observe that the qualitative nature of the critical point $\bar{B}_3$ is same as B_3, which has been described earlier, and therefore, the phase portrait will be the same as Fig. 6.

On the other hand, for $\nu < 0$, the algebraic curve represented by Eq. (33) has no branches in the positive quadrant. Hence, for $\nu < 0$, S does not have any critical points, that means, the autonomous system in this case has only three critical points, namely, $\bar{B}_0$, $\bar{B}_1$, $\bar{B}_2$ and the phase plot will be similar to Fig. 5.

C. Model III

In this section we describe the dynamical analysis for the interacting scenario driven by the interaction function

TABLE III. The critical points, their existence, stability, and the values of the cosmological parameters evaluated at those points for the interacting scenario driven by the interaction function $Q_{\rm III} = \Gamma(\rho_c - \rho_d - \frac{\rho_c\rho_d}{\rho_c+\rho_d})$ of Eq. (12) are summarized.

Point	x	z	Existence	Stability	Acceleration	Ω_c	Ω_d	$w_{\rm tot}$
C_0	$\frac{\sqrt{5}-1}{2}$	1	$\gamma(>0)$ and $w_d < -\frac{1}{3}$	$-\frac{3+\sqrt{5}}{2} < w_d < -\frac{1}{3}$	$w_d < -\frac{3+\sqrt{5}}{6}$	$\frac{\sqrt{5}-1}{2}$	$\frac{3-\sqrt{5}}{2}$	$\frac{w_d(3-\sqrt{5})}{2}$
C_1	0	0	$\gamma(>0)$ and $w_d < -\frac{1}{3}$	$w_d < -1$	$w_d < -\frac{1}{3}$	0	1	w_d
C_2	1	0	$\gamma(>0)$ and $w_d < -\frac{1}{3}$	Unstable	No	1	0	0
C_3	$\frac{1+w_d}{w_d}$	$\frac{3w_d(1+w_d)}{(3-\gamma)w_d^2+3w_d(1-\gamma)-\gamma}$	$\gamma(>0)$ and $-\frac{3+\sqrt{5}}{2} \le w_d \le -1$	Unstable	Yes	$\frac{1+w_d}{w_d}$	$-\frac{1}{w_d}$	-1

$Q_{\rm III}$ of (12). Using the same dynamical variables (x, z) defined as

$$x = \frac{\kappa^2\rho_c}{3H^2}, \qquad z = \frac{H_0}{H + H_0}, \tag{35}$$

the autonomous system for this interacting scenario takes the form

$$\begin{cases} x' = -\gamma\left(\frac{z}{1-z}\right)(x^2 + x - 1) + 3w_d x(1-x), \\ z' = \frac{3}{2}(1-z)z(1 + w_d(1-x)), \end{cases} \tag{36}$$

where $\gamma = \Gamma/H_0$ is the dimensionless parameter. Now, regularizing the vector fields, as we have described in III A, the autonomous system (36) can be reduced to the form

$$\begin{cases} x' = -\gamma z(x^2 + x - 1) + 3w_d(1-z)x(1-x), \\ z' = \frac{3}{2}(1-z)^2 z(1 + w_d(1-x)). \end{cases} \tag{37}$$

Here, $R = [0, 1]^2$ is the physical domain, and proceeding as earlier, we see that R will be positively invariant if we restrict the parameter γ by $\gamma > 0$ (i.e., $\Gamma > 0$). We, now, investigate the autonomous system (37) in terms of the nature of the critical points and their implications for both constant and dynamical w_d.

1. Constant w_d

For constant w_d, the critical points of the autonomous system (37), their existence, and stability, as well as the cosmological parameters evaluated at those critical points, are summarized in Table III. In the following we investigate the nature of the critical points for three different regions of w_d, namely, quintessence (i.e., $w_d > -1$), cosmological constant (i.e., $w_d = -1$), and phantom (i.e., $w_d < -1$).

(1) When $w_d > -1$, the point C_3 does not belong to the physical domain, and $w_{\rm tot} = w_d(1-x) > -1$, which means $z' = \frac{3}{2}z(1-z)^2(1 + w_{\rm tot}) > 0$. Now, on $z = 1$, x' is positive for $x < \frac{\sqrt{5}-1}{2}$, and x' is negative for $x > \frac{\sqrt{5}-1}{2}$. So, C_1, C_2 are unstable, and C_0 is a global attractor. Note that C_0 corresponds to $H = 0$, $\Omega_c = \frac{\sqrt{5}-1}{2}$, and $\Omega_d = \frac{3-\sqrt{5}}{2}$. The phase plot is displayed in Fig. 9.

(2) When $w_d = -1$, we have $C_1 = C_3$, and $z' = \frac{3}{2}z(1-z)^2 x$, which is positive. On $z = 1$ line, one has $x' > 0$ for $x < \frac{\sqrt{5}-1}{2}$ and $x' < 0$ for $x > \frac{\sqrt{5}-1}{2}$. Once again, C_1, C_2 are unstable critical points, and

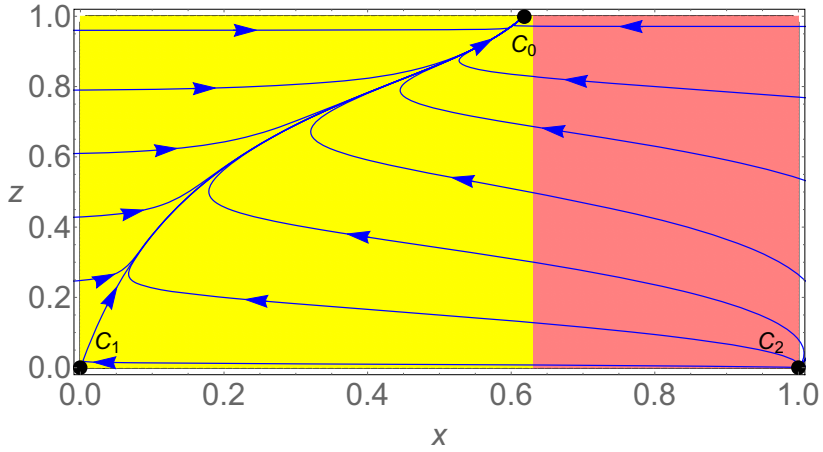

FIG. 9. Phase plot for model III [Eq. (12)] with $\gamma > 0$ and $w_d \ge -1$. In this case we have taken $w_d = -0.9$ and $\gamma = 0.5$. We note that one can take any value of $w_d \ge -1$ and any positive value of γ in order to get similar graphics. Here, the yellow shaded region represents the accelerated region (i.e., $q < 0$), and the pink shaded region corresponds to the decelerated region (i.e., $q > 0$).

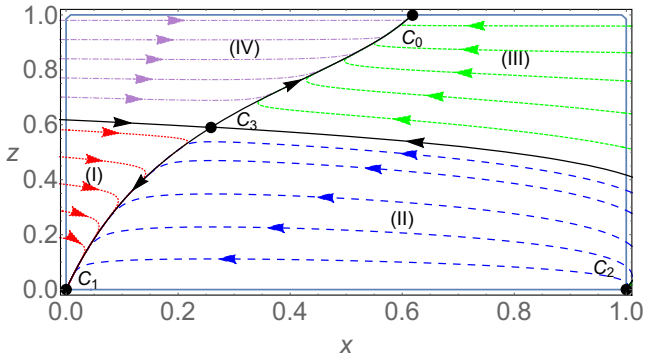

FIG. 10. Phase plot for model III [Eq. (12)] with $\gamma > 0$ and $-\frac{3+\sqrt{5}}{2} < w_d < -1$. In this case we have taken $w_d = -1.35$ and $\gamma = 0.8$. We note that one can take any specific value of $\gamma(> 0)$ to draw the plot, however, as long as γ decreases, regions I and IV become very small, and they look indistinguishable from one another.

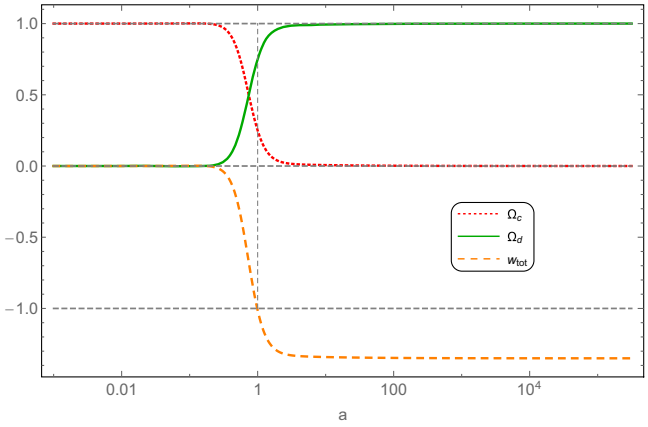

FIG. 11. We display the evolution of the CDM density parameter (Ω_c), dark energy density parameter (Ω_d), and the total equation of state parameter ($w_{\rm tot}$) for model III [Eq. (12)]. We have chosen the following values of the parameters: $w_d = -1.35$, $\gamma = 0.8$ and the following initial conditions: $x(N = 0) = 0.25$, $z(N = 0) = 0.07$ from region II of Fig. 10. In addition, if we start any trajectory from region I of Fig. 10, then it converges to the critical point C_1. So, for any initial conditions from region I, we shall get $\Omega_c = 0$ and $\Omega_d = 1$ at late time. Any trajectories starting from regions III and IV of Fig. 10 will converge to the critical point C_0. Therefore, if we take initial conditions on $x(N)$ and $z(N)$ from regions III and IV, we shall reach $\Omega_c = \frac{\sqrt{5}-1}{2}$ and $\Omega_d = \frac{3-\sqrt{5}}{2}$ in an asymptotic fashion.

the point C_0 continues being a global attractor. Again, the phase plot is shown in Fig. 9.

(3) For $w_d < -1$, the parameter space can be categorized in two ways:

(i) When $-\frac{\sqrt{5}+3}{2} < w_d < -1$, the point C_3 enters in the physical domain, and we obtain $0 < \frac{1+w_d}{w_d} < \frac{\sqrt{5}-1}{2}$. Now, if $x < \frac{1+w_d}{w_d}$, then that implies $1 + w_{\rm tot} < 0$, which gives $z' = \frac{3}{2}z(1-z)^2(1+w_{\rm tot}) < 0$. Similarly, $z' > 0$ for $x > \frac{1+w_d}{w_d}$. Again, on $z = 1$, we obtain $x' > 0$ for $x < \frac{\sqrt{5}-1}{2}$ and $x' < 0$ for $x > \frac{\sqrt{5}-1}{2}$. Also, x' is negative on $z = 0$. Thus, the physical region R is divided into four regions. Trajectories from regions I and II converge to C_1 and trajectories from regions III and IV converge to C_0. Figure 10 shows the qualitative nature and Fig. 11 displays the evolution of Ω_c, Ω_d, and $w_{\rm tot}$.

(ii) When $w_d \leq -\frac{\sqrt{5}+3}{2}$: For the special case with $w_d = -\frac{\sqrt{5}+3}{2}$, one has $C_0 = C_3$ and $\frac{1+w_d}{w_d} = \frac{\sqrt{5}-1}{2}$. Now, z' is positive for $x > \frac{1+w_d}{w_d}$, and z' is negative for $x < \frac{1+w_d}{w_d}$. On $z = 0$, x' is negative, which shows C_1 is a global attractor. Again for $w_d < -\frac{\sqrt{5}+3}{2}$, the point C_3 leaves the physical domain and one obtains $\frac{\sqrt{5}-1}{2} < \frac{1+w_d}{w_d} < 1$. Also, one has $z' > 0$ for $x > \frac{1+w_d}{w_d}$ and $z' < 0$ for $x < \frac{1+w_d}{w_d}$. Thus, C_1 is a global attractor. In this case, the qualitative behavior is given in Fig. 12.

2. Dynamical w_d

We consider the dynamical w_d of the form (23), for which the autonomous system (36) becomes

$$\begin{cases} x' = -\gamma\left(\frac{z}{1-z}\right)(x^2+x-1) - 3x(1-x)\left(1+\nu\frac{(1-z)^2(1-x)}{z^2}\right), \\ z' = \frac{3}{2}(1-z)z\left(x-\nu\frac{(1-z)^2(1-x)^2}{z^2}\right), \end{cases} \tag{38}$$

where $\nu = \frac{3AH_0^2}{\kappa^2}$. The topologically equivalent autonomous system after regularization is given by the following:

$$\begin{cases} x' = -\gamma z^3(x^2+x-1) - 3(1-z)x(1-x)(z^2+\nu(1-z)^2(1-x)), \\ z' = \frac{3}{2}(1-z)^2 z(xz^2 - \nu(1-z)^2(1-x)^2). \end{cases} \tag{39}$$

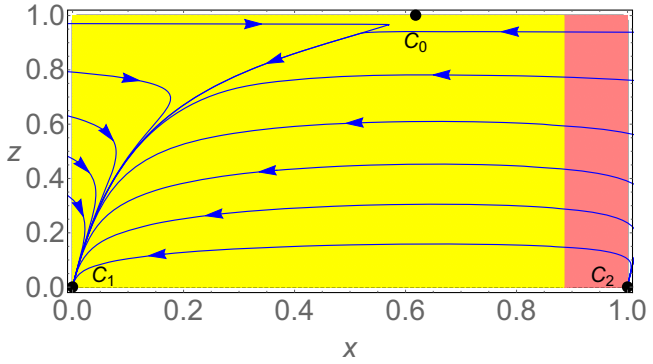

FIG. 12. Phase plot for model III [Eq. (12)] with $\gamma > 0$ and $w_d \leq -\frac{3+\sqrt{5}}{2}$. In this case we have taken $w_d = -2.9$ and $\gamma = 0.7$. We note that one can take any value of w_d satisfying $w_d \leq -\frac{3+\sqrt{5}}{2}$ and any positive value of γ in order to get similar graphics. Here, the yellow shaded region represents the accelerated region (i.e., $q < 0$), and the pink shaded region corresponds to the decelerated region (i.e., $q > 0$).

The critical points of the system (39) are

$$\bar{C}_0 = \left(\frac{\sqrt{5}-1}{2}, 1\right), \qquad \bar{C}_1 = (0,0),$$
$$\bar{C}_2 = (1,0), \qquad S = \left\{\left(x_c, \frac{3x_c}{3x_c - \gamma({x_c}^2 + x_c - 1)}\right)\right\},$$

where S is the set of critical points in which x_c is a real root of $g(x) \equiv 9x^3 - \gamma^2\nu(x^2 + x - 1)^2(1-x)^2 = 0$.[7] Note that as $g(x)$ is a sixth degree equation, therefore, the set S may have maximum six critical points. Thus, it is now important to calculate the number of critical points in order to understand the phase space of the interacting scenario for this dynamical w_d. As $g(0) = -\gamma^2\nu < 0$ (for $\nu > 0$) and $g(1) = 9 > 0$, it follows by the Bolzano's theorem [169] that $g(x)$ has at least one real root in (0, 1). Now, for any x_c lying in (0, 1), the condition $z_c = \frac{3x_c}{3x_c - \gamma({x_c}^2 + x_c - 1)} \leq 1$ requires $x_c \leq \frac{\sqrt{5}-1}{2}$. We also observe that $g(\frac{\sqrt{5}-1}{2}) = 9(-2+\sqrt{5}) > 0$, and hence, from the Bolzano's theorem [169], there is at least one root of $g(x)$ in $(0, \frac{\sqrt{5}-1}{2})$. We now claim that $g(x)$ has only one root in the interval $[0, \frac{\sqrt{5}-1}{2}]$, and in that case, it is straightforward to conclude that there is only one critical point in the set S. Now, from the derivative of $g(x)$ given below,

$$g'(x) = -6\gamma^2\nu(x-1)\left(x - \sqrt{\frac{2}{3}}\right)\left(x + \sqrt{\frac{2}{3}}\right) \times \left(x - \frac{\sqrt{5}-1}{2}\right)\left(x + \frac{\sqrt{5}+1}{2}\right) + 27x^2,$$

we notice that $g'(x) > 0$ for $x \in (0, \frac{\sqrt{5}-1}{2})$, which means that $g(x)$ is strictly increasing in $(0, \frac{\sqrt{5}-1}{2})$. Therefore, the set S contains only one critical point, and we label this critical point as $\bar{C}_3$. In this case, the topological nature of the critical point $\bar{C}_3$ is the same as C_3 described earlier, and hence, the phase plot is the same as the Fig. 10.

On the other hand, looking at Eq. (40), and following the similar arguments as earlier for $\nu < 0$, we claim that the set S does not have any critical point for $\nu < 0$. Thus, in this case, we have only three critical points, namely, $\bar{C}_0$, $\bar{C}_1$, and, $\bar{C}_2$, and the phase portrait looks the same as Fig. 9.

D. Model IV

In this section we describe the dynamical analysis for the interaction function $Q_{\rm IV}$ of Eq. (13). Considering the (x, z) variables defined as

$$x = \frac{\kappa^2\rho_c}{3H^2}, \qquad z = \frac{H_0}{H + H_0}, \tag{42}$$

the autonomous system for this interaction model takes the form

$$\begin{cases} x' = -\left(\frac{z}{1-z}\right)(\alpha x - \beta x(1-x)) + 3w_d x(1-x), \\ z' = \frac{3}{2}z(1-z)(1 + w_d(1-x)), \end{cases} \tag{43}$$

where α, β are defined as $\alpha = \Gamma_c/H_0$, and $\beta = \Gamma_{cd}/H_0$, respectively, and they are dimensionless. Note again that $\alpha \neq \beta$ for the interaction model to be sign shifting. Here, we shall regularize the autonomous system (43) similar to the procedure we have applied in III A. The regularized autonomous system will be of the form

$$\begin{cases} x' = -z(\alpha x - \beta x(1-x)) + 3w_d(1-z)x(1-x), \\ z' = \frac{3}{2}z(1-z)^2(1 + w_d(1-x)). \end{cases} \tag{44}$$

Also we note that $R = [0,1]^2$ is the physical domain, and the lines $x = 0$, $z = 0$, $z = 1$ are invariant under the flow generated by the autonomous system (44). We also see that along the line $x = 1$, one obtains $x' = -\alpha z$. Hence, the physical domain R will be positively invariant if we restrict the parameter α by $\alpha > 0$ (i.e., $\Gamma_c > 0$). It has been mentioned in II A that the interaction function $Q_{\rm IV}$ will exhibit sign shifting property provided Γ_c and Γ_{cd} are of the same sign. Consequently, to be consistent with the positive invariance of the physical domain R and the sign shifting

[7] Here $g(x)$ can be obtained from the following two nullclines:

$$xz^2 - \nu(1-z)^2(1-x)^2 = 0, \tag{40}$$

$$-\gamma z^3(x^2 + x - 1) - 3x(1-x)(1-z)[z^2 + \nu(1-z)^2(1-x)] = 0. \tag{41}$$

TABLE IV. The critical points, their existence, stability, and the values of the cosmological parameters evaluated at those points for the interacting scenario driven by the interaction function $Q_{\rm IV} = \Gamma_c \rho_c - \Gamma_{cd} \frac{\rho_c \rho_d}{\rho_c + \rho_d}$ of Eq. (13) are summarized.

Point	x	z	Existence	Stability	Acceleration	Ω_c	Ω_d	$w_{\rm tot}$
D_0	$\frac{\beta-\alpha}{\beta}$	1	$\beta > \alpha > 0$ and $w_d < -\frac{1}{3}$	$-\frac{\beta}{\alpha} < w_d < -\frac{1}{3}$	$w_d < -\frac{\beta}{3\alpha}$	$\frac{\beta-\alpha}{\beta}$	$\frac{\alpha}{\beta}$	$\frac{\alpha w_d}{\beta}$
D_{00}	0	1	$\alpha > 0$, $\beta > 0$ and $w_d < -\frac{1}{3}$	$\alpha(>0) > \beta$ with $-1 < w_d < -\frac{1}{3}$	$w_d < -\frac{1}{3}$	0	1	w_d
D_1	0	0	$\alpha > 0$, $\beta > 0$ and $w_d < -\frac{1}{3}$	$w_d < -1$	$w_d < -\frac{1}{3}$	0	1	w_d
D_2	1	0	$\alpha > 0$, $\beta > 0$ and $w_d < -\frac{1}{3}$	Unstable	No	1	0	0
D_3	$\frac{1+w_d}{w_d}$	$-\frac{3w_d}{(\alpha-3)w_d+\beta}$	$\beta > \alpha > 0$ with $-\frac{\beta}{\alpha} \leq w_d \leq -1$	Unstable for $w_d \neq -1$	Yes	$\frac{1+w_d}{w_d}$	$-\frac{1}{w_d}$	-1

nature of the interaction function $Q_{\rm IV}$, we will restrict our attention here on $\alpha > 0$, $\beta > 0$.

In the following we investigate the nature of the critical points and their implications for the constant and non-constant nature of w_d.

1. Constant w_d

In this section we explore the nature of the critical points for different regions of w_d. In Table IV, we summarize the critical points of the autonomous system (44), their existence, and stability, as well as the cosmological parameters evaluated at those critical points. In the following we investigate the nature of the critical points for three different regions of w_d, namely, quintessence (i.e., $w_d > -1$), cosmological constant (i.e., $w_d = -1$), and phantom (i.e., $w_d < -1$).

(i) When $\beta > \alpha > 0$, the following situations arise:

(1) $w_d > -1$: When $w_d > -1$, the point D_3 does not belong to the physical region R and also $w_{\rm tot} = w_d(1-x) > -1$, which implies $z' = \frac{3}{2} z(1-z)^2 \times (1 + w_{\rm tot}) > 0$. In addition as $\beta > \alpha > 0$, the point D_0 enters in the region R. On $z = 1$ line, the value of x' is positive if $x < \frac{\beta-\alpha}{\beta}$, and x' is negative if $x > \frac{\beta-\alpha}{\beta}$. So, D_{00}, D_1, and D_2 are unstable critical points, and D_0 is a global attractor. At the point D_0, we have $H = 0$, $\Omega_c = \frac{\beta-\alpha}{\beta}$ and $\Omega_d = \frac{\alpha}{\beta}$. The left plot of Fig. 13 shows the behavior.

(2) $w_d = -1$: When $w_d = -1$, all points in the OZ axis are critical points, and also point D_3 lies on the OZ axis. Again, one gets $z' = \frac{3}{2} z(1-z)^2 x$, which is positive. At $z = 1$, one has $x' > 0$ for $x < \frac{\beta-\alpha}{\beta}$, and $x' < 0$ for $x > \frac{\beta-\alpha}{\beta}$. In this case, D_0 is an attractor, but it is not a global attractor. The qualitative nature is displayed in right plot of Fig. 13.

(3) When $-\frac{\beta}{\alpha} < w_d < -1$: The critical point D_3 enters in the physical domain. We have $0 < \frac{1+w_d}{w_d} < \frac{\beta-\alpha}{\beta}$. At $z = 0$, $x' = 3w_d x(1-x)$, which is negative, and at $z = 1$, we obtain $x' > 0$ for $x < \frac{\beta-\alpha}{\beta}$ and $x' < 0$ for $x > \frac{\beta-\alpha}{\beta}$. If

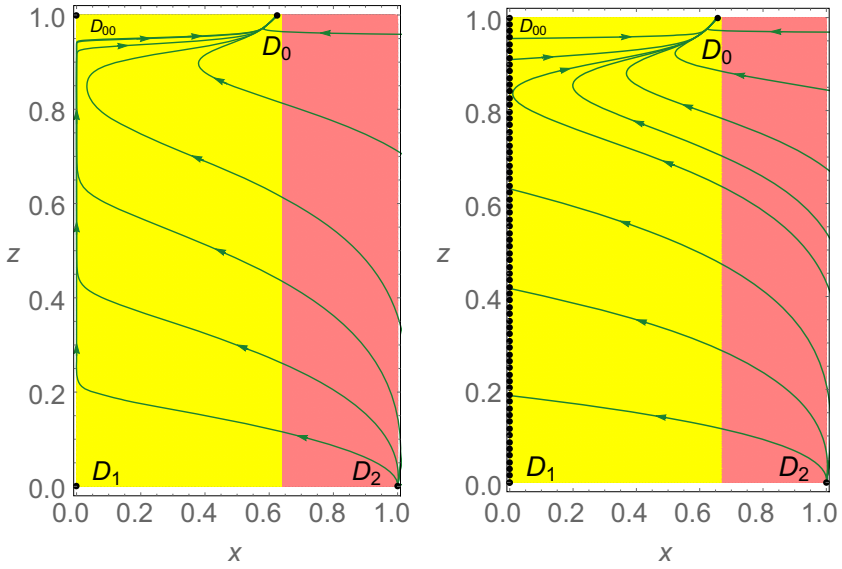

FIG. 13. Left plot: phase plot for model IV [Eq. (13)] with $w_d > -1$ and $\beta > \alpha > 0$. In this case we have used $w_d = -0.92$, $\alpha = 0.3$, and $\beta = 0.8$. Right plot: phase plot for model IV [Eq. (13)] with $w_d = -1$ and $\beta > \alpha > 0$. Particularly, we have taken $w_d = -1$, $\alpha = 0.31$, and $\beta = 0.9$. We note that the yellow shaded region represents the accelerated region (i.e., $q < 0$), and the pink shaded region corresponds to the decelerated region (i.e., $q > 0$).

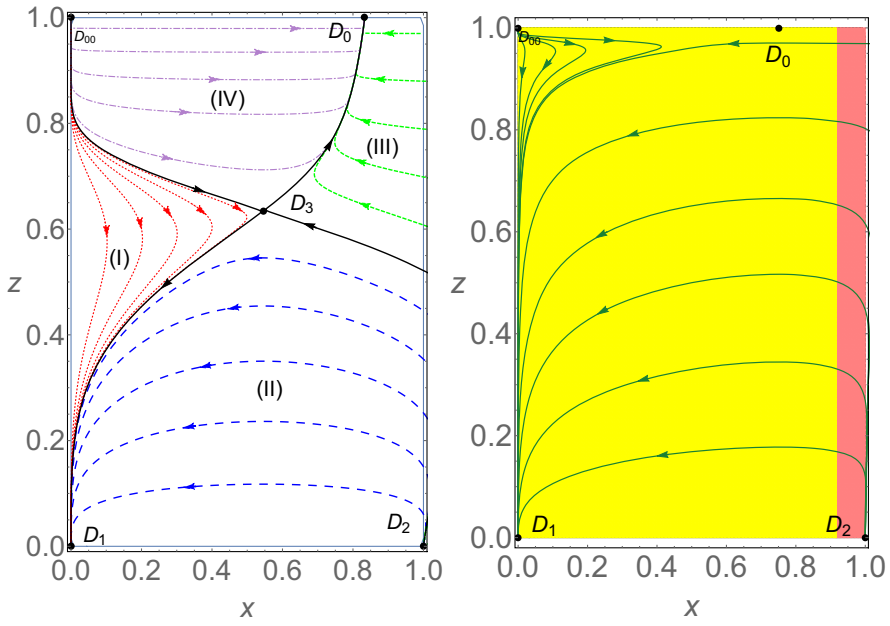

FIG. 14. Left plot: phase plot for model IV [Eq. (13)] with $-\frac{\beta}{\alpha} < w_d < -1$ and $\beta > \alpha > 0$. For numerical simulation we have used $w_d = -2.2$, $\alpha = 1$, and $\beta = 6$. Right plot: phase plot for model IV [Eq. (13)] with $w_d \leq -\frac{\beta}{\alpha}$ and $\beta > \alpha > 0$. For numerical simulation, we have used $w_d = -4.1$, $\alpha = 0.2$, and $\beta = 0.8$ from the parameter space. In this plot, the yellow shaded region corresponds to the accelerated region (i.e., $q < 0$), and the pink shaded region corresponds to the decelerated region (i.e., $q > 0$).

$x < \frac{1+w_d}{w_d}$, then it implies $1 + w_{\rm tot} < 0$. So, z' is negative. Similarly, z' is positive for $x > \frac{1+w_d}{w_d}$. Thus, all orbits in regions I and II of the left plot of Fig. 14, at late time, converge to D_1. For an orbit in regions III and IV of the left plot Fig. 14, at late time, it converges to D_0. Note that D_0 means $H = 0$ with $\Omega_c = \frac{\beta-\alpha}{\beta}, \Omega_d = \frac{\alpha}{\beta}$ and $w_{\rm tot} = \frac{\alpha w_d}{\beta} > -1$. On the contrary, D_1 means $H = \infty$ with $\Omega_d = 1$ and $w_{\rm tot} = w_d < -1$. Figure 15 presents the evolution of Ω_c, Ω_d, and $w_{\rm tot}$.

(4) $w_d \leq -\frac{\beta}{\alpha}$: When $w_d = -\frac{\beta}{\alpha}$, one obtains $D_0 = D_3$. Now, one has $z' < 0$ for $x < \frac{1+w_d}{w_d}$ and $z' > 0$ for $x > \frac{1+w_d}{w_d}$. Also, x' is negative on $z = 0$. Thus, D_1 is a global attractor. For $w_d < -\frac{\beta}{\alpha}$, the critical point D_3 leaves the physical region, and one gets $\frac{\beta-\alpha}{\beta} < \frac{1+w_d}{w_d} < 1$, which gives $z' < 0$ for $x < \frac{1+w_d}{w_d}$ and $z' > 0$ for $x > \frac{1+w_d}{w_d}$. Here also, we have $x' < 0$ on $z = 0$. Once again, D_1 is a global attractor. The right plot of Fig. 14 exhibits the phase plot.

(ii) $\alpha > \beta > 0$: In this case the critical points D_0 and D_3 never belong to the physical domain.
When $w_d > -1$, z' is positive as $1 + w_{\rm tot} > 0$. At $z = 1$ line, x' is negative. Thus, D_{00} is a global attractor. The point D_{00} corresponds to $H = 0$, $\Omega_c = 0$ and $\Omega_d = 1$.

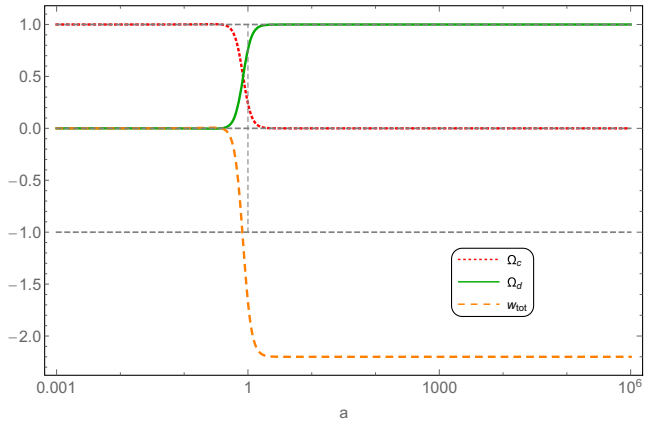

FIG. 15. We display the evolution of the CDM density parameter (Ω_c), dark energy density parameter (Ω_d), and the total equation of state parameter ($w_{\rm tot}$) for model IV [Eq. (13)]. We have chosen the following values of the parameters: $w_d = -2.2$, $\alpha = 1$, $\beta = 6$ and the following initial conditions: $x(N = 0) = 0.24$, $z(N = 0) = 0.01$ from region II of the left plot of Fig. 14. In addition, if we start any trajectory from region I of the left plot of Fig. 14, then it converges to the critical point D_1. So, for any initial conditions from region I, we shall get $\Omega_c = 0$ and $\Omega_d = 1$ at late time. Any trajectory starting from regions III and IV of the left plot of Fig. 14 will converge to the critical point D_0. Therefore, if we take initial conditions on $x(N)$ and $z(N)$ from regions III and IV, we shall reach $\Omega_c = \frac{\beta-\alpha}{\beta}$ and $\Omega_d = \frac{\alpha}{\beta}$ in an asymptotic fashion.

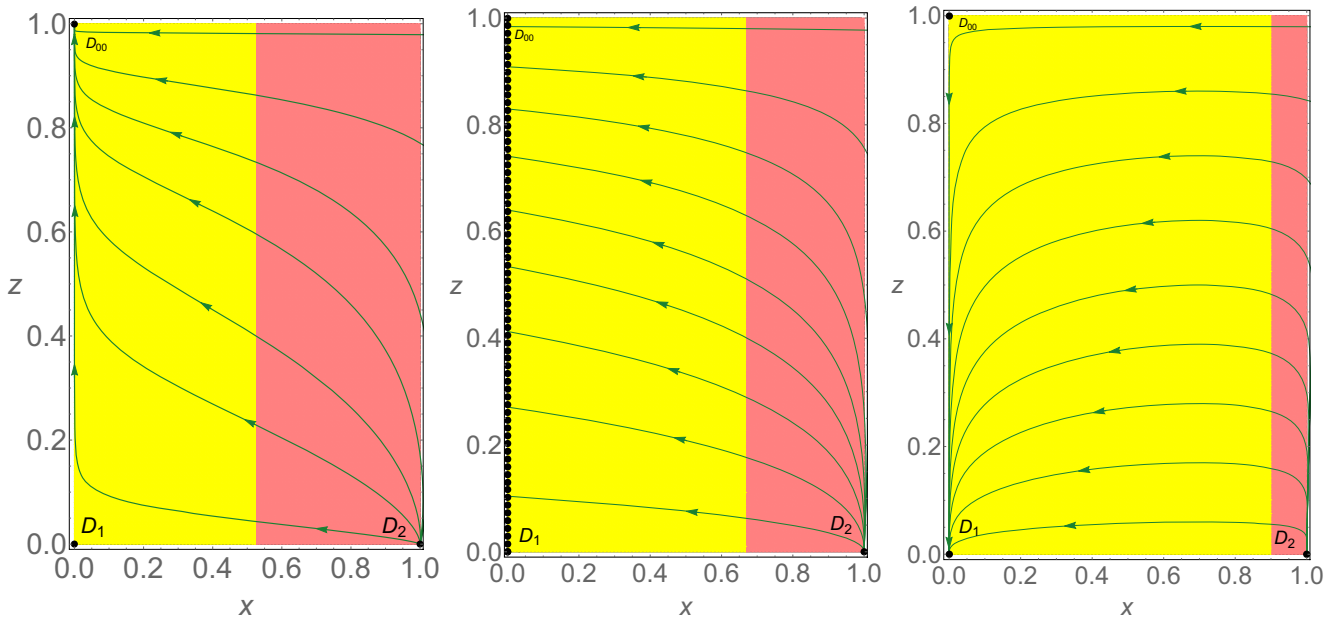

FIG. 16. Left plot: phase plot for model IV [Eq. (13)] with $w_d > -1$ and $\alpha > \beta > 0$. In this case we have used $w_d = -0.7$, $\alpha = 0.2$, and $\beta = 0.1$. Middle plot: phase plot for model IV [Eq. (13)] with $w_d = -1$ and $\alpha > \beta > 0$. Particularly, we have chosen $w_d = -1$, $\alpha = 0.08$, and $\beta = 0.05$. Right plot: phase plot for model IV [Eq. (13)] with $w_d < -1$ and $\alpha > \beta > 0$. For numerical simulation we have used $w_d = -3.3$, $\alpha = 0.2$, and $\beta = 0.1$. Here, the yellow shaded region represents the accelerated region (i.e., $q < 0$), and the pink shaded region corresponds to the decelerated region (i.e., $q > 0$).

When $w_d = -1$, all points in the OZ axis are critical points. Now, one has $z' = \frac{3}{2}z(1-z)^2x$, which is positive. Also, x' is negative on both $z = 0$ and $z = 1$ lines. Here, we have no attractor.
For $w_d < -1$, we have $0 < \frac{1+w_d}{w_d} < 1$. On $z = 0$ line, $x' = 3w_dx(1-x)$, which is negative. Here, we have $z' < 0$ for $x < \frac{1+w_d}{w_d}$ and $z' > 0$ for $x > \frac{1+w_d}{w_d}$. Thus, D_1 is the only global attractor. In all the cases, qualitative behaviors are shown in Fig. 16.

2. Dynamical w_d

For the equation of state (23), the autonomous system (43) becomes

$$\begin{cases} x' = -\left(\frac{z}{1-z}\right)x(\alpha-\beta(1-x)) - 3x(1-x)\left(1+\nu\frac{(1-z)^2(1-x)}{z^2}\right), \\ z' = \frac{3}{2}(1-z)z\left(x-\nu\frac{(1-z)^2(1-x)^2}{z^2}\right), \end{cases} \tag{45}$$

where $\nu = \frac{3AH_0^2}{\kappa^2}$. Proceeding as in the earlier cosmological models for nonconstant w_d, we regularize the autonomous system (45) and obtain the following:

$$\begin{cases} x' = -z^3x(\alpha-\beta(1-x)) - 3(1-z)x(1-x)(z^2+\nu(1-z)^2(1-x)), \\ z' = \frac{3}{2}(1-z)^2z(xz^2-\nu(1-z)^2(1-x)^2). \end{cases} \tag{46}$$

The critical points of the system (46) are

$$\bar{D}_0 = \left(\frac{\beta-\alpha}{\beta}, 1\right), \qquad \bar{D}_{00} = (0,1), \qquad \bar{D}_1 = (0,0), \qquad \bar{D}_2 = (1,0), \qquad S = \left\{\left(x_c, \frac{3}{3-\alpha+\beta(1-x_c)}\right)\right\},$$

where x_c is a root of $\Theta(x) \equiv 9x - \nu(-\alpha+\beta(1-x))^2(1-x)^2 = 0$.[8] Since $\Theta(x)$ represents a fourth degree equation in x,

[8]Note again that $\Theta(x)$ is obtained from the following two nullclines:

$$xz^2 - \nu(1-z)^2(1-x)^2 = 0, \tag{47}$$

$$-z^3x[\alpha-\beta(1-x)] - 3x(1-x)(1-z)[z^2+\nu(1-z)^2(1-x)] = 0. \tag{48}$$

therefore, S may contain a maximum of four critical points. In a similar fashion, we proceed to investigate the number of roots of $\Theta(x)$ in [0, 1]. Now, since $\Theta(0)=\nu(\beta-\alpha)^2<0$ (for $\nu>0$) and $\Theta(1)=9>0$, from the Bolzano's theorem [169], we can say that $\Theta(x)$ has at least one root in the interval (0, 1). However, as the physical domain in this case is R, therefore, for valid critical point in this domain, we have to check whether the z component of the critical point lies in [0, 1]. Now, for any x_c in [0, 1], the condition $\frac{3}{3-\alpha+\beta(1-x_c)}\leq 1$ demands that $\beta x_c\leq\beta-\alpha$. Now, as $\alpha>0$, $\beta>0$, we consider the following cases:

(i) $\beta>\alpha>0$: In this case, the condition $\beta x_c\leq\beta-\alpha$ reduces to $x_c\leq\frac{\beta-\alpha}{\beta}$. We see that $\Theta(0)<0$ and $\Theta(\frac{\beta-\alpha}{\beta})=9\frac{\beta-\alpha}{\beta}>0$, hence, from the Bolzano's theorem [169], there is at least one root of $\Theta(x)$ in $(0,\frac{\beta-\alpha}{\beta})$. We also observe that

$$\Theta'(x)=-4\beta^2\nu(x-1)\left(x-\frac{\beta-\alpha}{\beta}\right)\left(x-\frac{2\beta-\alpha}{2\beta}\right)+9>0,$$

for $x\in(0,\frac{\beta-\alpha}{\beta})$. Hence, $\Theta(x)$ is strictly increasing in $x\in(0,\frac{\beta-\alpha}{\beta})$, and as a result, $\Theta(x)$ has only one root in $x\in(0,\frac{\beta-\alpha}{\beta})$. Thus, the set S contains only one critical point, which we call as $\bar{D}_3$. The critical point $\bar{D}_3$ behaves qualitatively the same as the point D_3 and consequently, the phase portrait is topologically the same as the left plot of Fig. 14.

Again, following the same arguments as in the earlier models for $\nu<0$, we can show that $\Theta(x)$ has no root in (0, 1) for $\nu<0$. Hence, in this case the autonomous system has only four critical points, namely, $\bar{D}_0$, $\bar{D}_{00}$, $\bar{D}_1$, and $\bar{D}_2$. The phase space stability analysis has been shown before. The phase portrait is the same as the left plot of Fig. 13.

(ii) $\alpha>\beta>0$: In this case, we have $\beta-\alpha<0$, and hence, $\bar{D}_0$ does not belong to the physical domain R. Also, the condition $\beta x_c\leq\beta-\alpha$ leads to the claim that x_c does not belong to the domain [0, 1]. Therefore, we have only three critical points, $\bar{D}_{00}$, $\bar{D}_1$, and $\bar{D}_2$, and the phase portrait is the same as that of the phase portrait of the right plot of Fig. 16. On the other hand, for $\nu<0$, we do not have any critical point in S. Here, also, we have only three critical points, namely, $\bar{D}_{00}$, $\bar{D}_1$, and $\bar{D}_2$, and we see that the corresponding phase portrait looks similar to the left plot of Fig. 16.

E. Model V

In this section we discuss the dynamical analysis for the interacting scenario driven by the interaction function $Q_{\rm V}$ of Eq. (14). Using the dimensionless variables (x,z) defined as

$$x=\frac{\kappa^2\rho_c}{3H^2},\qquad z=\frac{H_0}{H+H_0},\tag{49}$$

we obtain the following autonomous system for the prescribed interacting scenario:

$$\begin{cases}x'=-\left(\frac{z}{1-z}\right)(1-x)(\alpha-\beta x)+3w_dx(1-x),\\ z'=\frac{3}{2}z(1-z)(1+w_d(1-x)),\end{cases}\tag{50}$$

where α, β are defined as $\alpha=\Gamma_d/H_0$ and $\beta=\Gamma_{cd}/H_0$, respectively, and $\alpha\neq\beta$. After regularizing, in a similar way we have performed in III A, the autonomous system (50) can be written of the form

$$\begin{cases}x'=-z(1-x)(\alpha-\beta x)+3w_d(1-z)x(1-x),\\ z'=\frac{3}{2}z(1-z)^2(1+w_d(1-x)).\end{cases}\tag{51}$$

The physical region is R, which is the square $R=[0,1]^2$, and following the similar arguments as in the case of earlier models, we observe that R is positively invariant if $\alpha<0$ (i.e., $\Gamma_d<0$). The interaction function $Q_{\rm V}$ as mentioned in (14) is of sign shifting nature provided that the coupling parameters Γ_d and Γ_{cd} are of the same sign. Hence, for the

TABLE V. The critical points, their existence, stability, and the values of the cosmological parameters evaluated at those points for the interacting scenario driven by the interaction function $Q_{\rm V}=\Gamma_d\rho_d-\Gamma_{cd}\frac{\rho_c\rho_d}{\rho_c+\rho_d}$ of Eq. (14) are summarized.

Point	x	z	Existence	Stability	Acceleration	Ω_c	Ω_d	$w_{\rm tot}$
E_0	$\frac{\alpha}{\beta}$	1	$\beta<\alpha<0$ and $w_d<-\frac{1}{3}$	$\frac{\beta}{\alpha-\beta}<w_d<-\frac{1}{3}$	$w_d<-\frac{1}{3}\frac{\beta}{\beta-\alpha}$	$\frac{\alpha}{\beta}$	$\frac{\beta-\alpha}{\beta}$	$\frac{(\beta-\alpha)w_d}{\beta}$
E_{00}	1	1	$\alpha<0$, $\beta<0$ and $w_d<-\frac{1}{3}$	$\alpha<\beta$ with $w_d<-\frac{1}{3}$	No	1	0	0
E_1	0	0	$\alpha<0$, $\beta<0$ and $w_d<-\frac{1}{3}$	$w_d<-1$	$w_d<-\frac{1}{3}$	0	1	w_d
E_2	1	0	$\alpha<0$, $\beta<0$ and $w_d<-\frac{1}{3}$	Unstable	No	1	0	0
E_3	$\frac{1+w_d}{w_d}$	$\frac{3w_d(1+w_d)}{3w_d^2+(\alpha-\beta+3)w_d-\beta}$	$\beta<\alpha<0$ with $\frac{\beta}{\alpha-\beta}\leq w_d\leq-1$ and $\alpha<\beta<0$ with $w_d\leq-1$	Unstable	Yes	$\frac{1+w_d}{w_d}$	$-\frac{1}{w_d}$	-1

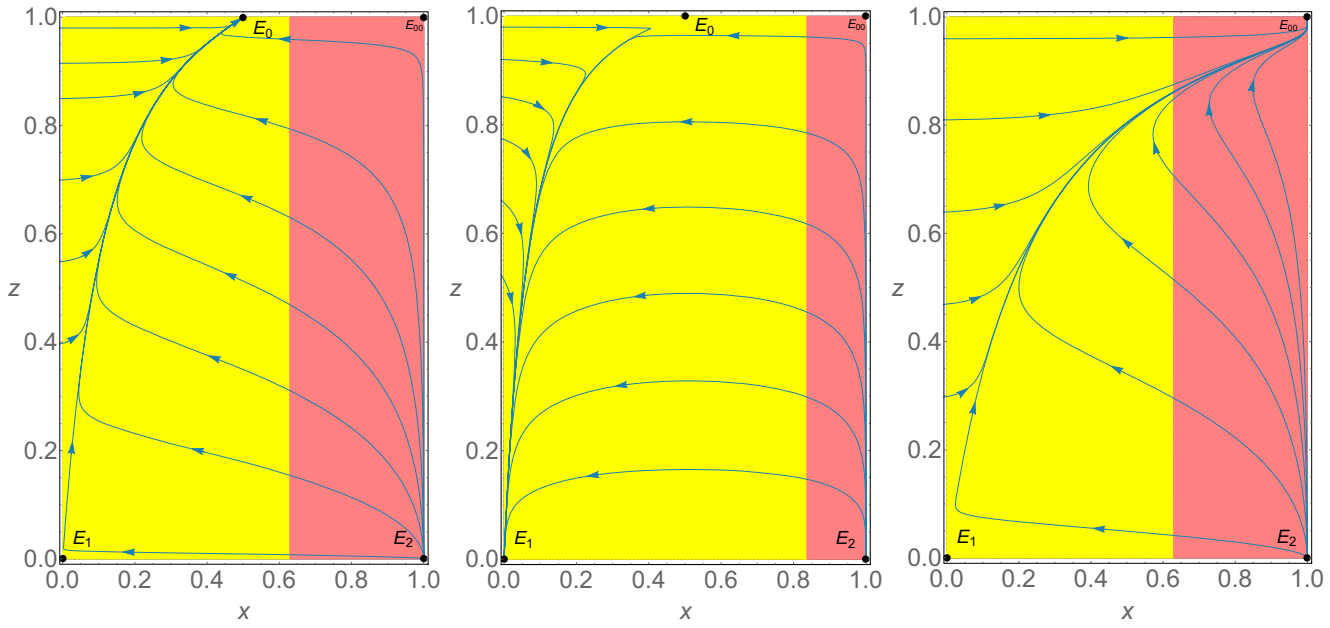

FIG. 17. Left plot: phase plot for model V [Eq. (14)] with $w_d \geq -1$ and $\beta < \alpha < 0$. In this case we have chosen $w_d = -0.9$, $\alpha = -0.3$, and $\beta = -0.6$. Middle plot: phase plot for model V [Eq. (14)] with $w_d \leq \frac{\beta}{\alpha-\beta}$ and $\beta < \alpha < 0$. In this case we have chosen $w_d = -2.05$, $\alpha = -0.3$, and $\beta = -0.6$. Right plot: phase plot for model V [Eq. (14)] with $w_d \geq -1$ and $\alpha < \beta < 0$. In this case we have chosen $w_d = -0.9$, $\alpha = -0.6$, and $\beta = -0.3$. Here, the yellow shaded region represents the accelerated region (i.e., $q < 0$), and the pink shaded region corresponds to the decelerated region (i.e., $q > 0$).

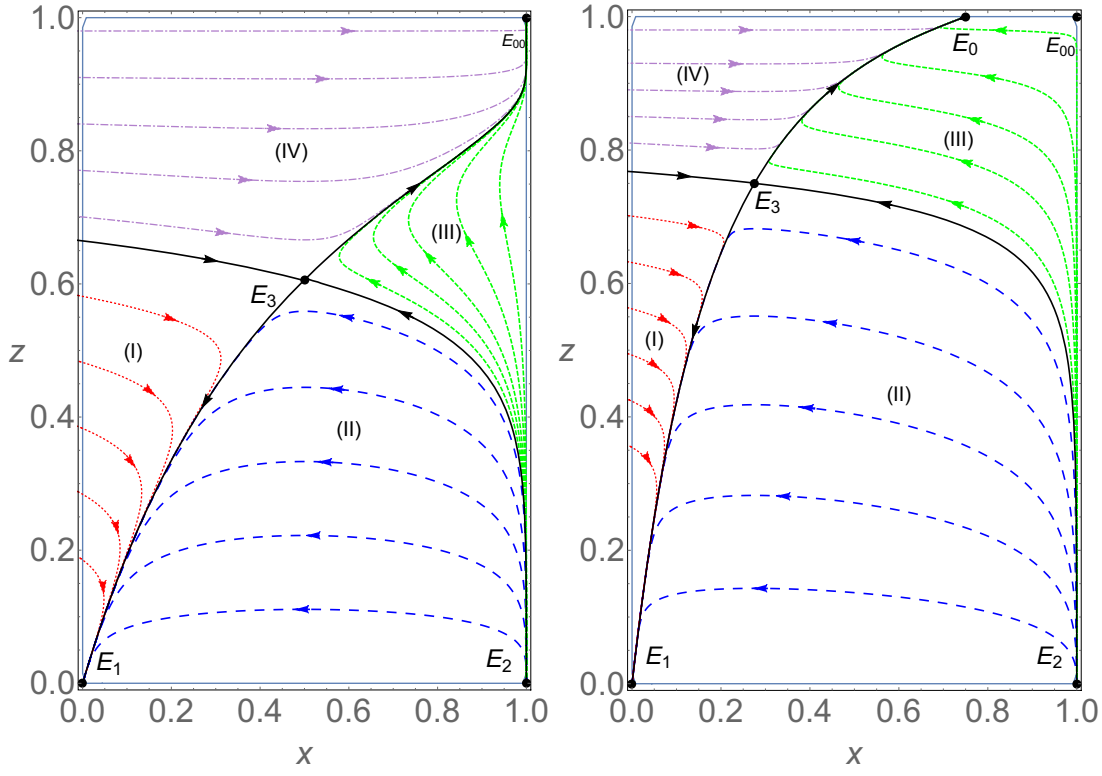

FIG. 18. Left plot: phase plot for model V [Eq. (14)] with $w_d < -1$ and $\alpha < \beta < 0$. In this case we have chosen $w_d = -2$, $\alpha = -2$, and $\beta = -0.1$. Right plot: phase plot for model V [Eq. (14)] with $\frac{\beta}{\alpha-\beta} < w_d < -1$ and $\beta < \alpha < 0$. In this case we have taken $w_d = -1.38$, $\alpha = -0.6$, and $\beta = -0.8$. We note that one can take any specific value of $\alpha(< 0)$ and $\beta(< 0)$ with $\beta < \alpha < 0$ to draw the plot, however, as long as α and β increase, regions I and IV become very small, and they look indistinguishable from one another.

dynamical analysis driven by the sign shifting interaction function Q_V, and to keep the physical domain R positively invariant, we assume the parametric condition $\alpha < 0, \beta < 0$.

1. Constant w_d

For constant w_d, the critical points of the autonomous system (51), their existence, and stability, as well as the cosmological parameters evaluated at those critical points are summarized in Table V. Similar to the earlier cases, here we consider various cases of w_d depending on its parameter space. In what follows we consider various cases.

(i) We consider the first case where the dimensionless coupling parameter satisfies the relation $\beta < \alpha < 0$:
  (1) When $w_d > -1$, E_3 leaves the domain R and one has $w_{\rm tot} = w_d(1-x) > -1$, which implies $z' > 0$. On $z = 1$ line, one gets $x' > 0$ for $x < \frac{\alpha}{\beta}$ and $x' < 0$ for $x > \frac{\alpha}{\beta}$. Thus, E_0 is a global attractor. The left plot of Fig. 17 shows the behavior.
  (2) For $w_d = -1$, one obtains $E_3 = E_1$ and $z' = \frac{3}{2}z(1-z)^2 x > 0$. On $z = 1$ line, one has $x' > 0$ for $x < \frac{\alpha}{\beta}$ and $x' < 0$ for $x > \frac{\alpha}{\beta}$. So, E_0 is a global attractor. Again, the phase plot is given in the left plot of Fig. 17.
  (3) When $\frac{\beta}{\alpha-\beta} < w_d < -1$, then E_3 enters in the physical region, and one can get $\frac{1+w_d}{w_d} < \frac{\alpha}{\beta}$. On $z = 0$, one obtains $x' < 0$. Also, on $z = 1$, one has $x' > 0$ for $x < \frac{\alpha}{\beta}$ and $x' < 0$ for $x > \frac{\alpha}{\beta}$. Again, z' is negative whenever $x < \frac{1+w_d}{w_d}$, and z' is positive whenever $x > \frac{1+w_d}{w_d}$. Thus, all orbits in regions I and II of the right plot of Fig. 18, at late time, converge to E_1. For an orbit in regions III and IV of the right plot of Fig. 18, at late time, it converges to E_0. In Fig. 19 we show the evolution of Ω_c, Ω_d, and $w_{\rm tot}$.
  (4) When $w_d = \frac{\beta}{\alpha-\beta}$, one can obtain $E_3 = E_0$, and x' is negative on $z = 0$. Also z' is negative for $x < \frac{1+w_d}{w_d}$, and z' is positive for $x > \frac{1+w_d}{w_d}$. Thus, E_1 is a global attractor. The qualitative behavior is displayed in the middle plot of Fig. 17.
  (5) When $w_d < \frac{\beta}{\alpha-\beta}$, E_3 leaves the physical domain and one has $\frac{1+w_d}{w_d} > \frac{\alpha}{\beta}$. As before, x' is negative on $z = 0$. Again, z' is negative in the left side of $x = \frac{1+w_d}{w_d}$, and z' is positive in the right side of $x = \frac{1+w_d}{w_d}$. Therefore, E_1 is a global attractor. The middle plot of Fig. 17 exhibits the qualitative nature.

(ii) We consider the case when the dimensionless coupling parameters satisfy $\alpha < \beta < 0$. In this case, E_0 leaves the domain as $\frac{\alpha}{\beta} > 1$. In the following we discuss the nature of the critical points for different values of w_d.
  (1) For $w_d > -1$, E_3 leaves the domain R. Now since $w_{\rm tot} = w_d(1-x) > -1$, hence, it implies that z' is positive. On $z = 1$ line, x' is positive. As a result, E_1, E_2 are unstable, and E_{00} is a global attractor. The right plot of Fig. 17 shows the qualitative behavior.
  (2) When $w_d = -1$, we obtain $E_1 = E_3$ and $z' = \frac{3}{2}z(1-z)^2 x$, which is positive. At $z = 1$ line, x' is positive. Thus, E_{00} is again a global attractor. The phase plot is displayed in the right plot of Fig. 17.
  (3) When $w_d < -1$, E_3 enters in the physical region R and for this w_d, we also have $0 < \frac{1+w_d}{w_d} < 1$. On $z = 0$ line, $x' = 3w_d x(1-x)$, which is negative, and on $z = 1$ line, x' is positive. Now in the left side of $x = \frac{1+w_d}{w_d}$, z' is negative, and in the right side of $x = \frac{1+w_d}{w_d}$, z' is positive. Hence, the physical region R is divided into four regions. Thus, all orbits in regions I and II of the left plot of Fig. 18, at late time, converge to E_1. For an orbit in regions III and IV of the left plot of Fig. 18, at late time, it converges to E_{00}.

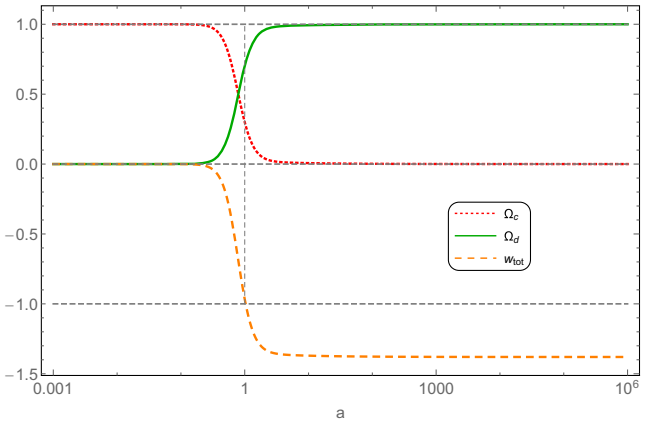

FIG. 19. We display the evolution of the CDM density parameter (Ω_c), dark energy density parameter (Ω_d), and the total equation of state parameter ($w_{\rm tot}$) for model V [Eq. (14)]. We have chosen the following values of the parameters: $w_d = -1.38$, $\alpha = -0.6$, $\beta = -0.8$ and the following initial conditions: $x(N=0) = 0.3$, $z(N=0) = 0.1$ from region II of the right plot of Fig. 18. In addition, if we start any trajectory from region I of the right plot of Fig. 18, it converges to the critical point E_1. So, for any initial conditions from region I, we shall get $\Omega_c = 0$ and $\Omega_d = 1$ at late time. Any trajectory starting from regions III and IV of the right plot of Fig. 18 will converge to the critical point E_0. Therefore, if we take initial conditions on $x(N)$ and $z(N)$ from regions III and IV, we shall reach $\Omega_c = \frac{\alpha}{\beta}$ and $\Omega_d = \frac{\beta-\alpha}{\beta}$ in an asymptotic fashion.

2. Dynamical w_d

We work with the same dynamical w_d of Eq. (23) for which the autonomous system (50) takes the form:

$$\begin{cases} x' = -\left(\frac{z}{1-z}\right)(1-x)(\alpha-\beta x) - 3x(1-x)\left(1+\nu\frac{(1-z)^2(1-x)}{z^2}\right), \\ z' = \frac{3}{2}(1-z)z\left(x-\nu\frac{(1-z)^2(1-x)^2}{z^2}\right), \end{cases} \tag{52}$$

where $\nu = \frac{3AH_0^2}{\kappa^2}$. Regularizing the autonomous system (52), we get

$$\begin{cases} x' = -z^3(1-x)(\alpha-\beta x) - 3(1-z)x(1-x)(z^2+\nu(1-z)^2(1-x)), \\ z' = \frac{3}{2}(1-z)^2 z(xz^2-\nu(1-z)^2(1-x)^2), \end{cases} \tag{53}$$

where the regularization amounts to the result that the autonomous systems (52) and (53) are topologically equivalent. The critical points of the system (53) are

$$\bar{E}_0 = \left(\frac{\alpha}{\beta}, 1\right), \qquad \bar{E}_{00} = (1,1), \qquad \bar{E}_1 = (0,0),$$

$$\bar{E}_2 = (1,0), \qquad S = \left\{\left(x_c, \frac{3x_c}{3x_c-(1-x_c)(\alpha-\beta x_c)}\right)\right\},$$

where S represents the set of critical points in which x_c is a root of $\Psi(x) \equiv 9x^3 - \nu(1-x)^4(\alpha-\beta x)^2 = 0$.[9] As $\Psi(x)$ represents a six degree equation in x, therefore, S may contain a maximum of six critical points. Now we see that $\Psi(0) = -\nu\alpha^2 < 0$ (for $\nu > 0$) and $\Psi(1) > 0$, therefore, from Bolzano's theorem [169], $\Psi(x)$ has at least one real root in the interval (0, 1). For real and physically meaningful critical points in our domain R, the z component of the critical point, i.e., $z_c = \frac{3x_c}{3x_c-(1-x_c)(\alpha-\beta x_c)}$, must belong to [0, 1]. Thus, for any $0 \le x_c \le 1$, the criterion $0 \le \frac{3x_c}{3x_c-(1-x_c)(\alpha-\beta x_c)} \le 1$ leads to the condition that $(\alpha-\beta x_c) \le 0$. Now, since $\alpha < 0$, $\beta < 0$, we consider the following cases:

(i) $\beta < \alpha < 0$: In this case, we have $0 \le x_c \le \alpha/\beta$. We also see that $\Psi(\alpha/\beta) = 9(\alpha/\beta)^3 > 0$. Consequently, we conclude from Bolzano's theorem [169] that there is at least one root of $\Psi(x)$ in $(0, \alpha/\beta)$. Now, from the derivative of $\Psi(x)$,

$$\Psi'(x) = -6\beta^2\nu(x-1)^3\left(x-\frac{\alpha}{\beta}\right)\left(x-\frac{2\alpha+\beta}{3\beta}\right) + 27x^2, \tag{56}$$

we notice that $\Psi'(x) > 0$ for $x \in (0, \alpha/\beta)$. Hence, the function $\Psi(x)$ is strictly increasing in $(0, \alpha/\beta)$, which finally concludes that there is only one root of $\Psi(x)$ in $(0, \alpha/\beta)$. Therefore, the set of critical points S contains only one critical point, and for convenience, we label this critical point as $\bar{E}_3$. In this case, the point $\bar{E}_3$ qualitatively behaves like the point E_3, which is described earlier, and correspondingly, the phase portrait looks the same as the right plot of Fig. 18.

On the other hand, for $\nu < 0$, following the earlier arguments, we can show that $\Psi(x)$ has no root in (0, 1). This shows that for $\nu < 0$, we have only four critical points: $\bar{E}_0$, $\bar{E}_{00}$, $\bar{E}_1$, and $\bar{E}_2$, and the phase plot is the same as the left plot of Fig. 17.

(ii) $\alpha < \beta < 0$: We already know that x_c satisfies the inequality $\alpha - \beta x_c \le 0$, but in contrary to the earlier case, in this parameter space, we have $\alpha/\beta > 1$, and consequently, the critical point $\bar{E}_0$ does not belong to the physical domain R. We now investigate the number of real roots of $\Psi(x)$ in the interval [0, 1] for $\nu > 0$ because for $\nu < 0$, as already commented, there is no root of $\Psi(x)$ in [0, 1]. Here, we see that $\frac{2\alpha+\beta}{3\beta} > 1$.[10] Now, looking at the expression for $\Psi'(x)$ in Eq. (56), we see that
$(x-1) < 0$ as $x \in (0,1)$,
$(x-\frac{\alpha}{\beta}) < 0$ in (0, 1) since $\frac{\alpha}{\beta} > 1$,
$(x-\frac{2\alpha+\beta}{3\beta}) < 0$ in (0, 1) as $\frac{2\alpha+\beta}{3\beta} > 1$,
therefore, $\Psi'(x)$ is always positive in (0, 1). Thus, $\Psi(x)$ being a strictly increasing function in (0, 1) has only one root in (0, 1). Hence, the set S contains only one critical point in the domain R. The phase space stability analysis of this critical point is the same as that of the critical point E_3, and the phase plot is the same as the left plot of Fig. 18.

[9]Note that $\Psi(x)$ is obtained from the following two nullclines:

$$xz^2 - \nu(1-z)^2(1-x)^2 = 0, \tag{54}$$

$$-z^3(1-x)[\alpha-\beta x] - 3x(1-x)(1-z)[z^2+\nu(1-z)^2(1-x)] = 0. \tag{55}$$

[10]One can check that $\frac{2\alpha+\beta}{3\beta} = \frac{2}{3}\left(\frac{\alpha}{\beta}\right) + \frac{1}{3} > \frac{2}{3} + \frac{1}{3} = 1$ (since $\alpha/\beta > 1$).

As before, the polynomial $\Psi(x)$ has no real root in the interval [0, 1] for $\nu < 0$. Therefore, in this case, we will have only three critical points: $\bar{E}_{00}$, $\bar{E}_1$, and $\bar{E}_2$, and the phase plot will be similar to the right plot of Fig. 17.

IV. SUMMARY AND CONCLUDING REMARKS

Cosmology with nongravitational interaction between DM and DE is the theme of this work. This particular theory, according to the existing records, has occupied a very decent place in the list of alternative cosmological models beyond ΛCDM. In this article we have raised some important questions regarding some not so usual constraints on the interaction functions and performed a detailed phase space analysis of the interacting scenarios featuring some novel qualities that distinguish with the existing works in this direction. According to the existing records in the literature, in almost every interacting scenario, some common (but not so natural) assumptions are considered, such as, the flow of energy should be either from DE to DM or in the reverse direction, that means either DE will be gainer or DM will be gainer. The question arises why such unidirectional property of the interaction function should be obeyed given the fact that the nature of the interaction function is still an open question to the astrophysics and the cosmology community? On the other hand, there are ceaseless debates on the choice of the interaction functions—whether the interaction functions should involve the (global) expansion rate explicitly or not. Moreover, in the context of the DE fluid, should we consider its equation of state to be dynamical or constant?

Considering these debates, in this work we have considered the following setup: (i) the assumption of unidirectional interaction functions have been generalized by means of some sign shifting interaction functions, which recover the unidirectional interaction functions as a special case, and thus, in this new picture of interacting dynamics, we allow the bidirectional energy flow; (ii) the interaction functions do not depend on the external parameters of the Universe, rather, they depend on the intrinsic nature of the dark components, and hence, they are expected to offer inherent nature of the dark sector at the fundamental level, and in addition, (iii) along with the constant DE equation of state, we have considered a dynamical parametrization of the DE equation of state belonging to the class (22), which adds a new ingredient in this context, and, so far as we are aware of the existing literature, this is the first time we are reporting such analysis.

We begin the study by considering a very simple but elegant linear interaction function $Q_{\rm I} = \Gamma(\rho_c - \rho_d)$ of (10) and then considered its linear and nonlinear extensions in terms of other interaction functions given in Eqs. (11)–(14). With the choice of suitable dimensionless variables (this is very crucial in the analysis, since for some specific choices of the variables, one may not obtain all the critical points of the system), we have obtained all the critical points of the interacting scenarios. The detailed analyses of the interacting scenarios for both constant and dynamical w_d are described in Secs. III A–III E. Tables I–V summarize the critical points, their existence, stability, and the values of the key cosmological parameters, and in Figs. 1–19, we have shown the nature of the critical points and the evolution of some key cosmological parameters. For the sake of convenience, an overall summary of results extracted out of all the sign shifting interacting scenarios is given in Table VI, where mainly the nature of the critical points for the present sign shifting interacting scenarios has been shown for different nature of the DE equation of state.

Focusing on the constant DE equation of state, w_d, we found that each sign shifting interacting scenario admits a variety of critical points which are qualitatively different, namely, the matter dominated critical point which is unstable in nature; late time stable attractors corresponding to an accelerating expansion of the Universe in which one stable attractor is completely DE dominated (i.e., $\Omega_d = 1$), and in one attractor both DE and DM exist, and hence, this attractor is physically more interesting according to the present observational results. Moreover, we found that all the sign shifting interacting scenarios also admit global attractors for different regions of the DE equation of state, namely, $w_d > -1$ (nonphantom), $w_d = -1$ (cosmological constant), and $w_d < -1$ (phantom), see Table VI. At this point, it is important to mention that the sign shifting nature of the interaction functions can affect the space of critical points. In particularly, there is a connection between the late time stable attractors and the present sign shifting interaction functions because if this sign shifting nature of the present interaction functions is replaced by the unidirectional interaction functions that means when the transfer of energy between the dark components is restricted to only in one direction,[11] then the late time stable attractors, namely, A_0, B_0, C_0, D_0, and E_0 do not appear within these unidirectional interaction functions. However, in the proposed sign shifting interaction models, A_0, B_0, C_0, D_0, and E_0 appear at the transitional point where $Q(\rho_c, \rho_d)$ changes its sign. It is an interesting feature of the proposed sign shifting interacting models, and it is a subject for further investigations.

The case with dynamical DE equation of state presents a more general interacting scenario. The present choice of w_d

[11]If the interaction functions $Q_{\rm I} = \Gamma(\rho_c - \rho_d)$ and $Q_{\rm III} = \Gamma(\rho_c - \rho_d - \frac{\rho_c\rho_d}{\rho_c+\rho_d})$ are replaced by $\tilde{Q}_{\rm I} = \Gamma(\rho_c + \rho_d)$ and $\tilde{Q}_{\rm III} = \Gamma(\rho_c + \rho_d + \frac{\rho_c\rho_d}{\rho_c+\rho_d})$, respectively, (note that $\tilde{Q}_{\rm I}$ and $\tilde{Q}_{\rm III}$ represent unidirectional interaction functions), then the critical points A_0, C_0 do not appear in these new unidirectional interacting scenarios. In a similar fashion, for $Q_{\rm II}$, $Q_{\rm IV}$, and $Q_{\rm V}$, if we impose that the coupling parameters will have the opposite signs instead of the same signs, which are essential for the sign shifting nature, then the late time stable attractors B_0, D_0, and E_0 do not appear in the respective unidirectional interacting scenario.

TABLE VI. Summary table describing all the interaction functions, the critical points, and their nature for both constant and dynamical DE equation of state.

Constant w_d						
		Stability of critical points				
Interaction models	Critical points	Attractor	Global attractor	Repeller	Deceleration parameter (q)	Figures
$Q_{\mathrm{I}} = \Gamma(\rho_c - \rho_d)$	A_0, A_1 A_2, A_3	A_0, A_1 are attractors If $-2 < w_d < -1$ and $\gamma > 0$	A_0 is a global attractor For $w_d \geq -1$ and $\gamma > 0$; A_1 is a global attractor for $w_d \leq -2$ and $\gamma > 0$	A_0: $w_d \leq -2$, $\gamma > 0$ A_1: $w_d \geq -1$, $\gamma > 0$ A_2: always ($\gamma > 0$) A_3: $-2 \leq w_d \leq -1$, $\gamma > 0$	$q(A_0) = \frac{1}{2}(1 + \frac{3w_d}{2}) < 0$ If $w_d < -2/3$; $q(A_1) = \frac{1}{2}(1 + 3w_d) < 0$ If $w_d < -1/3$; $q(A_2) = 1/2$; $q(A_3) = -1$	Figures 1–4
$Q_{\mathrm{II}} = \Gamma_c\rho_c - \Gamma_d\rho_d$	B_0, B_1 B_2, B_3	B_0, B_1 are attractors For $-(1 + \frac{\beta}{\alpha}) < w_d < -1$, $\alpha > 0$ and $\beta > 0$	B_0 is a global attractor For $w_d \geq -1$, $\alpha > 0$ and $\beta > 0$; B_1 is a global attractor for $w_d \leq -(1 + \frac{\beta}{\alpha})$, $\alpha > 0$ and $\beta > 0$	For $\alpha > 0$ and $\beta > 0$ B_0: $w_d \leq -(1 + \frac{\beta}{\alpha})$ B_1: $w_d \geq -1$ B_2: always B_3: $-(1 + \frac{\beta}{\alpha}) \leq w_d \leq -1$	$q(B_0) = \frac{1}{2}(1 + \frac{3\alpha w_d}{\alpha+\beta}) < 0$ If $w_d < -\frac{1}{3}(1 + \frac{\beta}{\alpha})$; $q(B_1) = \frac{1}{2}(1 + 3w_d) < 0$ If $w_d < -1/3$; $q(B_2) = 1/2$; $q(B_3) = -1$	Figures 5–8
$Q_{\mathrm{III}} = \Gamma(\rho_c - \rho_d - \frac{\rho_c\rho_d}{\rho_c+\rho_d})$	C_0, C_1 C_2, C_3	C_0, C_1 are attractors For $-(3 + \sqrt{5})/2 < w_d < -1$ and $\gamma > 0$	C_0 is a global attractor For $w_d \geq -1$ and $\gamma > 0$; C_1 is a global attractor for $w_d \leq -(3 + \sqrt{5})/2$	For $\gamma > 0$ C_0: $w_d \leq -(3 + \sqrt{5})/2$ C_1: $w_d \geq -1$ C_2: always C_3: $-(3 + \sqrt{5})/2 \leq w_d \leq -1$	$q(C_0) = \frac{1}{2}(1 + \frac{3w_d(3-\sqrt{5})}{2}) < 0$ If $w_d < -(3 + \sqrt{5})/6$; $q(C_1) = \frac{1}{2}(1 + 3w_d) < 0$ If $w_d < -1/3$; $q(C_2) = 1/2$; $q(C_3) = -1$	Figures 9–12
$Q_{\mathrm{IV}} = \Gamma_c\rho_c - \Gamma_{cd}\frac{\rho_c\rho_d}{\rho_c+\rho_d}$	D_0, D_{00}, D_1, D_2, D_3	D_0 is an attractor If $-\beta/\alpha < w_d \leq -1$ And $\beta > \alpha > 0$; D_1 is an attractor If $-\beta/\alpha < w_d < -1$ And $\beta > \alpha > 0$	D_0 is a global attractor If $w_d > -1$ and $\beta > \alpha > 0$; D_1 is a global attractor If $w_d \leq -\beta/\alpha$ with $\beta > \alpha > 0$ And if $w_d < -1$ with $\alpha > \beta > 0$; D_{00} is a global attractor If $w_d > -1$ and $\alpha > \beta > 0$	For $\beta > \alpha > 0$ D_0: $w_d \leq -\beta/\alpha$ D_{00}: $w_d \neq -1$ D_1: $w_d > -1$ D_2: always D_3: $-\beta/\alpha \leq w_d < -1$ For $\alpha > \beta > 0$ D_{00}: $w_d < -1$ D_1: $w_d > -1$ D_2: always	$q(D_0) = \frac{1}{2}(1 + \frac{3\alpha w_d}{\beta}) < 0$ If $w_d < -\frac{\beta}{3\alpha}$; $q(D_{00}) = \frac{1}{2}(1 + 3w_d) < 0$ If $w_d < -1/3$; $q(D_1) = \frac{1}{2}(1 + 3w_d) < 0$ If $w_d < -1/3$; $q(D_2) = 1/2$; $q(D_3) = -1$	Figures 13–16

(Table continued)

TABLE VI. *(Continued)*

Constant w_d						
		Stability of critical points				
Interaction models	Critical points	Attractor	Global attractor	Repeller	Deceleration parameter (q)	Figures
$Q_V = \Gamma_d\rho_d - \Gamma_{cd}\frac{\rho_c\rho_d}{\rho_c+\rho_d}$				For $\beta < \alpha < 0$		
	E_0, E_{00}	E_0, E_1 are attractors	E_0 is a global attractor	E_0: $w_d \leq \beta/(\alpha-\beta)$	$q(E_0) = \frac{1}{2}(1+3w_d(1-\frac{\alpha}{\beta})) < 0$	
	E_1, E_2,	If $\beta/(\alpha-\beta)$ $< w_d < -1$	If $w_d \geq -1$ with $\beta < \alpha < 0$;	E_{00}: always	If $w_d < -\frac{1}{3}\frac{\beta}{\beta-\alpha}$;	Figures 17–19
	E_3	With $\beta < \alpha < 0$; E_{00}, E_1 are attractors	E_1 is a global attractor If $w_d \leq \beta/(\alpha-\beta)$ and $\beta < \alpha < 0$;	E_1: $w_d \geq -1$ E_2: always	$q(E_{00}) = 1/2$; $q(E_1) = \frac{1}{2}(1+3w_d) < 0$	
		If $w_d < -1$ with $\alpha < \beta < 0$	E_{00} is a global attractor	E_3: $\beta/(\alpha-\beta) \leq w_d \leq -1$	If $w_d < -1/3$;	
			If $w_d \geq -1$ with $\alpha < \beta < 0$	For $\alpha < \beta < 0$ E_1: $w_d \geq -1$ E_2: always E_3: $w_d \leq -1$	$q(E_2) = 1/2$; $q(E_3) = -1$	

Dynamical w_d						
		Stability of critical points				
Interaction models	Critical points	Attractor	Global attractor	Repeller	Deceleration parameter (q)	Figures
$Q_I = \Gamma(\rho_c - \rho_d)$				$\bar{A}_1$: $\nu < 0$ and $\gamma > 0$	$q(\bar{A}_0) = -1/4$;	
	$\bar{A}_0$, $\bar{A}_1$ $\bar{A}_2$, $\bar{A}_3$	$\bar{A}_0$, $\bar{A}_1$ are attractors If $\nu > 0$ and $\gamma > 0$	$\bar{A}_0$ is a global attractor If $\nu < 0$ and $\gamma > 0$	$\bar{A}_2$: always ($\gamma > 0$) $\bar{A}_3$: $\nu > 0$ and $\gamma > 0$	$q(\bar{A}_1) \longrightarrow -\infty$ if $\nu > 0$ And $q(\bar{A}_1) \longrightarrow +\infty$ if $\nu < 0$; $q(\bar{A}_2) = 1/2$; $q(\bar{A}_3) = -1$	Figures 1 and 2
$Q_{II} = \Gamma_c\rho_c - \Gamma_d\rho_d$					$q(\bar{B}_0) = \frac{1}{2}(\frac{\beta-2\alpha}{\alpha+\beta}) < 0$	
	$\bar{B}_0$, $\bar{B}_1$ $\bar{B}_2$, $\bar{B}_3$	$\bar{B}_0$, $\bar{B}_1$ are attractors If $\nu > 0$, $\alpha > 0$ and $\beta > 0$	$\bar{B}_0$ is a global attractor If $\nu < 0$, $\alpha > 0$ and $\beta > 0$	$\bar{B}_1$: $\nu < 0$, $\alpha > 0$ and $\beta > 0$ $\bar{B}_2$: always ($\alpha > 0$, $\beta > 0$) $\bar{B}_3$: $\nu > 0$, $\alpha > 0$ and $\beta > 0$	If $\beta < 2\alpha$; $q(\bar{B}_1) \longrightarrow -\infty$ if $\nu > 0$ And $q(\bar{B}_1) \longrightarrow +\infty$ if $\nu < 0$; $q(\bar{B}_2) = 1/2$; $q(\bar{B}_3) = -1$	Figures 5 and 6

(Table continued)

TABLE VI. *(Continued)*

		Dynamical w_d				
		Stability of critical points				
Interaction models	Critical points	Attractor	Global attractor	Repeller	Deceleration parameter (q)	Figures
$Q_{\mathrm{III}} = \Gamma(\rho_c - \rho_d - \frac{\rho_c\rho_d}{\rho_c+\rho_d})$	$\bar{C}_0$, $\bar{C}_1$ $\bar{C}_2$, $\bar{C}_3$	$\bar{C}_0$, $\bar{C}_1$ are attractors If $\nu > 0$ and $\gamma > 0$	$\bar{C}_0$ is a global attractor If $\nu < 0$ and $\gamma > 0$	$\bar{C}_1$: $\nu < 0$ and $\gamma > 0$ $\bar{C}_2$: always ($\gamma > 0$) $\bar{C}_3$: $\nu > 0$ and $\gamma > 0$	$q(\bar{C}_0) = \frac{3\sqrt{5}-7}{4} < 0$; $q(\bar{C}_1) \longrightarrow -\infty$ if $\nu > 0$ And $q(\bar{C}_1) \longrightarrow +\infty$ if $\nu < 0$; $q(\bar{C}_2) = 1/2$; $q(\bar{C}_3) = -1$	Figures 9 and 10
$Q_{\mathrm{IV}} = \Gamma_c\rho_c - \Gamma_{cd}\frac{\rho_c\rho_d}{\rho_c+\rho_d}$	$\bar{D}_0$, $\bar{D}_{00}$, $\bar{D}_1$, $\bar{D}_2$, $\bar{D}_3$	$\bar{D}_0$, $\bar{D}_1$ are attractors If $\nu > 0$ and $\beta > \alpha > 0$	$\bar{D}_0$ is a global attractor If $\nu < 0$ and $\beta > \alpha > 0$; $\bar{D}_{00}$ is a global attractor If $\nu < 0$ and $\alpha > \beta > 0$; $\bar{D}_1$ is a global attractor If $\nu > 0$ and $\alpha > \beta > 0$	$\bar{D}_{00}$: $\nu \neq 0$ and $\beta > \alpha > 0$ $\bar{D}_1$: $\nu < 0$ and $\beta > \alpha > 0$ $\bar{D}_2$: always ($\beta > \alpha > 0$) $\bar{D}_3$: $\nu > 0$ and $\beta > \alpha > 0$ $\bar{D}_{00}$: $\nu > 0$ and $\alpha > \beta > 0$ $\bar{D}_1$: $\nu < 0$ and $\alpha > \beta > 0$ $\bar{D}_2$: always ($\alpha > \beta > 0$)	$q(\bar{D}_0) = \frac{\beta-3\alpha}{2\beta} < 0$ If $\beta < 3\alpha$; $q(\bar{D}_{00}) = -1$; $q(\bar{D}_1) \longrightarrow -\infty$ if $\nu > 0$ And $q(\bar{D}_1) \longrightarrow +\infty$ if $\nu < 0$; $q(\bar{D}_2) = 1/2$; $q(\bar{D}_3) = -1$	Figures 13, 14, and 16
$Q_{\mathrm{V}} = \Gamma_d\rho_d - \Gamma_{cd}\frac{\rho_c\rho_d}{\rho_c+\rho_d}$	$\bar{E}_0$, $\bar{E}_{00}$ $\bar{E}_1$, $\bar{E}_2$, $\bar{E}_3$	$\bar{E}_0$, $\bar{E}_1$ are attractors If $\nu > 0$ with $\beta < \alpha < 0$; $\bar{E}_{00}$, $\bar{E}_1$ are attractors If $\nu > 0$ with $\alpha < \beta < 0$	$\bar{E}_0$ is a global attractor If $\nu < 0$ with $\beta < \alpha < 0$; $\bar{E}_{00}$ is a global attractor If $\nu < 0$ with $\alpha < \beta < 0$	$\bar{E}_{00}$: always ($\beta < \alpha < 0$) $\bar{E}_1$: $\nu < 0$ with $\beta < \alpha < 0$ $\bar{E}_2$: always ($\beta < \alpha < 0$) $\bar{E}_3$: $\nu > 0$ with $\beta < \alpha < 0$ $\bar{E}_1$: $\nu < 0$ with $\alpha < \beta < 0$ $\bar{E}_2$: always ($\alpha < \beta < 0$) $\bar{E}_3$: $\nu > 0$ with $\alpha < \beta < 0$	$q(\bar{E}_0) = \frac{3\alpha-2\beta}{2\beta} < 0$ If $3\alpha > 2\beta$; $q(\bar{E}_{00}) = 1/2$; $q(\bar{E}_1) \longrightarrow -\infty$ if $\nu > 0$ And $q(\bar{E}_1) \longrightarrow +\infty$ if $\nu < 0$; $q(\bar{E}_2) = 1/2$; $q(\bar{E}_3) = -1$	Figures 17 and 18

[Eq. (23)] covers both the phantom (for $A > 0$, equivalently, $\nu > 0$) and nonphantom (for $A < 0$, equivalently, $\nu < 0$) regimes. In terms of the number of critical points, each sign shifting interacting model with dynamical phantom case (i.e., $\nu > 0$) has one extra critical point compared to the corresponding sign shifting interacting model with dynamical quintessence case ($\nu < 0$). Again, similar to the constant w_d case, here too, we observe that if the sign shifting nature of the interaction functions is replaced by the unidirectional interaction functions, then the late time stable attractors, namely, $\bar{A}_0$, $\bar{B}_0$, $\bar{C}_0$, $\bar{D}_0$, and $\bar{E}_0$ do not appear in this case, but in the context of the proposed sign shifting interaction models these late time stable attractors arise at the transitional point, that means where $Q(\rho_c, \rho_d)$ changes its sign. Specifically, we have the following observations:

(1) Dynamical phantom: In all the sign shifting interacting dynamical phantom scenarios, we find one matter dominated era (unstable in nature) representing a decelerating phase, late time stable attractors in which one attractor is completely DE dominated ($\Omega_d = 1$), and the other attractor allows the concurrence of DE and DM. Moreover, we noticed that only model IV in this series admits one global attractor $\bar{D}_1$ provided that the dimensionless coupling parameters satisfy $\alpha > \beta > 0$. According to the existing literature on the interacting dynamical phantom scenarios [18,19,147,155] concurrent existence of the matter dominated, only DE dominated ($\Omega_d = 1$), and the coexistence of DE and DM ($\Omega_d \neq 0, \Omega_c \neq 0$), as we observed within the context of present sign shifting interacting models, is very rare. For example, even though some specific interacting models exhibit the matter dominated phase [147,155], but the simultaneous occurrence of the DE dominated stable attractor ($\Omega_d = 1$), and the stable late time scaling attractor corresponding to an accelerating phase of the Universe has not been found.

(2) Dynamical quintessence: We find that all the scenarios in this category admit the matter dominated phase, which is unstable in nature, and it corresponds to a past decelerating phase. But, unlike in the phantom interacting scenario, here only one late time stable attractor is allowed, which is global in nature (see Table VI), and this critical point allows the existence of both DE and DM. The existence of the matter dominated phase within the present sign shifting models is interesting because such phase is not so common in a variety of interaction models when w_d lies in the quintessence regime, see, for instance, [19,27,146,148,153].

Based on the outcomes of the present article, it is evident that the sign shifting interaction models are quite appealing. The results further emphasize that there should not be any particular reason to prefer only the unidirectional interaction functions in the context of interacting DE, rather, the bidirectional interaction functions are quite promising, and they deserve further attention. Specifically, the analysis with dynamical w_d within these interaction models is very promising, but such analysis is rare in the literature.

ACKNOWLEDGMENTS

The authors thank the referees for their time to read our article and for giving some useful comments that helped us to improve the article. S. H. acknowledges the financial support from the University Grants Commission (UGC), Govt. of India (NTA Ref. No: 201610019097). J. d. H. is supported by the Spanish Grant No. PID2021-123903NB-I00 funded by MCIN/AEI/10.13039/501100011033 and by "ERDF A way of making Europe." T. S. and S. P. acknowledge the financial support from the Department of Science and Technology (DST), Govt. of India under the Scheme "Fund for Improvement of S&T Infrastructure (FIST)" (File No. SR/FST/MS-I/2019/41).

[1] A. G. Riess *et al.* (Supernova Search Team), Observational evidence from supernovae for an accelerating universe and a cosmological constant, Astron. J. **116**, 1009 (1998).

[2] S. Perlmutter *et al.* (Supernova Cosmology Project Collaboration), Measurements of Ω and Λ from 42 high redshift supernovae, Astrophys. J. **517**, 565 (1999).

[3] E. J. Copeland, M. Sami, and S. Tsujikawa, Dynamics of dark energy, Int. J. Mod. Phys. D **15**, 1753 (2006).

[4] J. Frieman, M. Turner, and D. Huterer, Dark energy and the accelerating universe, Annu. Rev. Astron. Astrophys. **46**, 385 (2008).

[5] K. Bamba, S. Capozziello, S. Nojiri, and S. D. Odintsov, Dark energy cosmology: The equivalent description via different theoretical models and cosmography tests, Astrophys. Space Sci. **342**, 155 (2012).

[6] S. Nojiri and S. D. Odintsov, Introduction to modified gravity and gravitational alternative for dark energy, eConf **C0602061**, 06 (2006).

[7] S. Nojiri and S. D. Odintsov, Unified cosmic history in modified gravity: From F(R) theory to Lorentz non-invariant models, Phys. Rep. **505**, 59 (2011).
[8] A. De Felice and S. Tsujikawa, f(R) theories, Living Rev. Relativity **13**, 3 (2010).
[9] S. Capozziello and M. De Laurentis, Extended theories of gravity, Phys. Rep. **509**, 167 (2011).
[10] T. Clifton, P. G. Ferreira, A. Padilla, and C. Skordis, Modified gravity and cosmology, Phys. Rep. **513**, 1 (2012).
[11] K. Koyama, Cosmological tests of modified gravity, Rep. Prog. Phys. **79**, 046902 (2016).
[12] Y.-F. Cai, S. Capozziello, M. De Laurentis, and E. N. Saridakis, f(T) teleparallel gravity and cosmology, Rep. Prog. Phys. **79**, 106901 (2016).
[13] S. Nojiri, S. D. Odintsov, and V. K. Oikonomou, Modified gravity theories on a nutshell: Inflation, bounce and late-time evolution, Phys. Rep. **692**, 1 (2017).
[14] Y. Akrami *et al.* (CANTATA Collaboration), *Modified Gravity and Cosmology: An Update by the CANTATA Network*, edited by E. N. Saridakis, R. Lazkoz, V. Salzano, P. Vargas Moniz, S. Capozziello, J. Beltrán Jiménez, M. De Laurentis, and G. J. Olmo (Springer, New York, 2021).
[15] S. Bahamonde, K. F. Dialektopoulos, C. Escamilla-Rivera, G. Farrugia, V. Gakis, M. Hendry, M. Hohmann, J. Levi Said, J. Mifsud, and E. Di Valentino, Teleparallel gravity: From theory to cosmology, Rep. Prog. Phys. **86**, 026901 (2023).
[16] L. Amendola, Coupled quintessence, Phys. Rev. D **62**, 043511 (2000).
[17] L. Amendola and C. Quercellini, Tracking and coupled dark energy as seen by WMAP, Phys. Rev. D **68**, 023514 (2003).
[18] Z.-K. Guo, R.-G. Cai, and Y.-Z. Zhang, Cosmological evolution of interacting phantom energy with dark matter, J. Cosmol. Astropart. Phys. 05 (2005) 002.
[19] B. Gumjudpai, T. Naskar, M. Sami, and S. Tsujikawa, Coupled dark energy: Towards a general description of the dynamics, J. Cosmol. Astropart. Phys. 06 (2005) 007.
[20] R.-G. Cai and A. Wang, Cosmology with interaction between phantom dark energy and dark matter and the coincidence problem, J. Cosmol. Astropart. Phys. 03 (2005) 002.
[21] B. Wang, C.-Y. Lin, and E. Abdalla, Constraints on the interacting holographic dark energy model, Phys. Lett. B **637**, 357 (2006).
[22] J. D. Barrow and T. Clifton, Cosmologies with energy exchange, Phys. Rev. D **73**, 103520 (2006).
[23] M. S. Berger and H. Shojaei, An interacting dark energy model for the expansion history of the Universe, Phys. Rev. D **74**, 043530 (2006).
[24] M. R. Setare, Interacting holographic dark energy model and generalized second law of thermodynamics in non-flat universe, J. Cosmol. Astropart. Phys. 01 (2007) 023.
[25] R. Rosenfeld, Reconstruction of interacting dark energy models from parameterizations, Phys. Rev. D **75**, 083509 (2007).
[26] C. Feng, B. Wang, Y. Gong, and R.-K. Su, Testing the viability of the interacting holographic dark energy model by using combined observational constraints, J. Cosmol. Astropart. Phys. 09 (2007) 005.
[27] C. G. Boehmer, G. Caldera-Cabral, R. Lazkoz, and R. Maartens, Dynamics of dark energy with a coupling to dark matter, Phys. Rev. D **78**, 023505 (2008).
[28] G. Olivares, F. Atrio-Barandela, and D. Pavon, The integrated Sachs-Wolfe effect in interacting dark energy models, Phys. Rev. D **77**, 103520 (2008).
[29] J. Valiviita, E. Majerotto, and R. Maartens, Instability in interacting dark energy and dark matter fluids, J. Cosmol. Astropart. Phys. 07 (2008) 020.
[30] H. Mohseni Sadjadi and N. Vadood, Notes on interacting holographic dark energy model in a closed universe, J. Cosmol. Astropart. Phys. 08 (2008) 036.
[31] N. Cruz, S. Lepe, F. Pena, and J. Saavedra, Holographic dark energy interacting with dark matter in a closed Universe, Phys. Lett. B **669**, 271 (2008).
[32] S. Wang and Y. Zhang, Alleviation of cosmic age problem in interacting dark energy model, Phys. Lett. B **669**, 201 (2008).
[33] G. Caldera-Cabral, R. Maartens, and L. A. Urena-Lopez, Dynamics of interacting dark energy, Phys. Rev. D **79**, 063518 (2009).
[34] M. B. Gavela, D. Hernandez, L. Lopez Honorez, O. Mena, and S. Rigolin, Dark coupling, J. Cosmol. Astropart. Phys. 07 (2009) 034; 05 (2010) E01.
[35] G. Caldera-Cabral, R. Maartens, and B. M. Schaefer, The growth of structure in interacting dark energy models, J. Cosmol. Astropart. Phys. 07 (2009) 027.
[36] J. Valiviita, R. Maartens, and E. Majerotto, Observational constraints on an interacting dark energy model, Mon. Not. R. Astron. Soc. **402**, 2355 (2010).
[37] L. Lopez Honorez, B. A. Reid, O. Mena, L. Verde, and R. Jimenez, Coupled dark matter-dark energy in light of near Universe observations, J. Cosmol. Astropart. Phys. 09 (2010) 029.
[38] F. Yu, J. Zhang, J. Lu, W. Wang, and Y. Gui, A more general interacting model of holographic dark energy, Phys. Lett. B **688**, 263 (2010).
[39] H. Wei, Revisiting the cosmological constraints on the interacting dark energy models, Phys. Lett. B **691**, 173 (2010).
[40] I. Duran, D. Pavon, and W. Zimdahl, Observational constraints on a holographic, interacting dark energy model, J. Cosmol. Astropart. Phys. 07 (2010) 018.
[41] X. Chen, B. Wang, N. Pan, and Y. Gong, Constraining the interacting dark energy models from weak gravity conjecture and recent observations, Phys. Lett. B **695**, 30 (2011).
[42] S. Cao, N. Liang, and Z.-H. Zhu, Testing the phenomenological interacting dark energy with observational $H(z)$ data, Mon. Not. R. Astron. Soc. **416**, 1099 (2011).
[43] T. Clemson, K. Koyama, G.-B. Zhao, R. Maartens, and J. Valiviita, Interacting dark energy—constraints and degeneracies, Phys. Rev. D **85**, 043007 (2012).
[44] F. Marulli, M. Baldi, and L. Moscardini, Clustering and redshift-space distortions in interacting dark energy cosmologies, Mon. Not. R. Astron. Soc. **420**, 2377 (2012).

[45] M. Baldi and P. Salucci, Constraints on interacting dark energy models from galaxy Rotation Curves, J. Cosmol. Astropart. Phys. 02 (2012) 014.
[46] J.-H. He, B. Wang, and E. Abdalla, Deep connection between f(R) gravity and the interacting dark sector model, Phys. Rev. D **84**, 123526 (2011).
[47] P. P. Avelino and H. M. R. da Silva, Effective dark energy equation of state in interacting dark energy models, Phys. Lett. B **714**, 6 (2012).
[48] T. Harko and F. S. N. Lobo, Irreversible thermodynamic description of interacting dark energy-dark matter cosmological models, Phys. Rev. D **87**, 044018 (2013).
[49] C.-Y. Sun and R.-H. Yue, Stable large-scale perturbations in interacting dark-energy model, J. Cosmol. Astropart. Phys. 08 (2013) 018.
[50] L. P. Chimento, M. G. Richarte, and I. E. Sánchez García, Interacting dark sector with variable vacuum energy, Phys. Rev. D **88**, 087301 (2013).
[51] Y.-H. Li and X. Zhang, Large-scale stable interacting dark energy model: Cosmological perturbations and observational constraints, Phys. Rev. D **89**, 083009 (2014).
[52] W. Yang and L. Xu, Cosmological constraints on interacting dark energy with redshift-space distortion after Planck data, Phys. Rev. D **89**, 083517 (2014).
[53] W. Yang and L. Xu, Testing coupled dark energy with large scale structure observation, J. Cosmol. Astropart. Phys. 08 (2014) 034.
[54] W. Yang and L. Xu, Coupled dark energy with perturbed Hubble expansion rate, Phys. Rev. D **90**, 083532 (2014).
[55] Y.-H. Li, J.-F. Zhang, and X. Zhang, Parametrized post-Friedmann framework for interacting dark energy, Phys. Rev. D **90**, 063005 (2014).
[56] N. Tamanini, Phenomenological models of dark energy interacting with dark matter, Phys. Rev. D **92**, 043524 (2015).
[57] R. S. Goncalves, G. C. Carvalho, and J. S. Alcaniz, Low-z test for interacting dark energy, Phys. Rev. D **92**, 123504 (2015).
[58] S. Pan, S. Bhattacharya, and S. Chakraborty, An analytic model for interacting dark energy and its observational constraints, Mon. Not. R. Astron. Soc. **452**, 3038 (2015).
[59] W. Yang, H. Li, Y. Wu, and J. Lu, Cosmological constraints on coupled dark energy, J. Cosmol. Astropart. Phys. 10 (2016) 007.
[60] R. C. Nunes, S. Pan, and E. N. Saridakis, New constraints on interacting dark energy from cosmic chronometers, Phys. Rev. D **94**, 023508 (2016).
[61] W. Yang, N. Banerjee, and S. Pan, Constraining a dark matter and dark energy interaction scenario with a dynamical equation of state, Phys. Rev. D **95**, 123527 (2017); **96**, 089903(A) (2017).
[62] J. Dutta, W. Khyllep, and N. Tamanini, Scalar-fluid interacting dark energy: Cosmological dynamics beyond the exponential potential, Phys. Rev. D **95**, 023515 (2017).
[63] E. Di Valentino, A. Melchiorri, and O. Mena, Can interacting dark energy solve the H_0 tension?, Phys. Rev. D **96**, 043503 (2017).
[64] L. Santos, W. Zhao, E. G. M. Ferreira, and J. Quintin, Constraining interacting dark energy with CMB and BAO future surveys, Phys. Rev. D **96**, 103529 (2017).
[65] J. Mifsud and C. Van De Bruck, Probing the imprints of generalized interacting dark energy on the growth of perturbations, J. Cosmol. Astropart. Phys. 11 (2017) 001.
[66] W. Yang, S. Pan, and D. F. Mota, Novel approach toward the large-scale stable interacting dark-energy models and their astronomical bounds, Phys. Rev. D **96**, 123508 (2017).
[67] M. S. Linton, A. Pourtsidou, R. Crittenden, and R. Maartens, Variable sound speed in interacting dark energy models, J. Cosmol. Astropart. Phys. 04 (2018) 043.
[68] W. Yang, S. Pan, and J. D. Barrow, Large-scale stability and astronomical constraints for coupled dark-energy models, Phys. Rev. D **97**, 043529 (2018).
[69] W. Yang, L. Xu, H. Li, Y. Wu, and J. Lu, Testing the interacting dark energy model with cosmic microwave background anisotropy and observational Hubble data, Entropy **19**, 327 (2017).
[70] W. Yang, S. Pan, E. Di Valentino, R. C. Nunes, S. Vagnozzi, and D. F. Mota, Tale of stable interacting dark energy, observational signatures, and the H_0 tension, J. Cosmol. Astropart. Phys. 09 (2018) 019.
[71] R. von Marttens, L. Casarini, D. F. Mota, and W. Zimdahl, Cosmological constraints on parametrized interacting dark energy, Phys. Dark Universe **23**, 100248 (2019).
[72] W. Yang, A. Mukherjee, E. Di Valentino, and S. Pan, Interacting dark energy with time varying equation of state and the H_0 tension, Phys. Rev. D **98**, 123527 (2018).
[73] C. Li, X. Ren, M. Khurshudyan, and Y.-F. Cai, Implications of the possible 21-cm line excess at cosmic dawn on dynamics of interacting dark energy, Phys. Lett. B **801**, 135141 (2020).
[74] S. Mishra and S. Chakraborty, Stability analysis of an interacting holographic dark energy model, Mod. Phys. Lett. A **34**, 19 (2019).
[75] S. Pan, W. Yang, E. Di Valentino, E. N. Saridakis, and S. Chakraborty, Interacting scenarios with dynamical dark energy: Observational constraints and alleviation of the H_0 tension, Phys. Rev. D **100**, 103520 (2019).
[76] E. Di Valentino, A. Melchiorri, O. Mena, and S. Vagnozzi, Interacting dark energy in the early 2020s: A promising solution to the H_0 and cosmic shear tensions, Phys. Dark Universe **30**, 100666 (2020).
[77] R. von Marttens, L. Lombriser, M. Kunz, V. Marra, L. Casarini, and J. Alcaniz, Dark degeneracy I: Dynamical or interacting dark energy?, Phys. Dark Universe **28**, 100490 (2020).
[78] G. Cheng, Y.-Z. Ma, F. Wu, J. Zhang, and X. Chen, Testing interacting dark matter and dark energy model with cosmological data, Phys. Rev. D **102**, 043517 (2020).
[79] S. Pan, G. S. Sharov, and W. Yang, Field theoretic interpretations of interacting dark energy scenarios and recent observations, Phys. Rev. D **101**, 103533 (2020).
[80] S. Pan, J. de Haro, W. Yang, and J. Amorós, Understanding the phenomenology of interacting dark energy scenarios and their theoretical bounds, Phys. Rev. D **101**, 123506 (2020).
[81] E. Di Valentino, A. Melchiorri, O. Mena, S. Pan, and W. Yang, Interacting dark energy in a closed universe, Mon. Not. R. Astron. Soc. **502**, L23 (2021).

[82] J. Beltrán Jiménez, D. Bettoni, D. Figueruelo, F. A. Teppa Pannia, and S. Tsujikawa, Velocity-dependent interacting dark energy and dark matter with a Lagrangian description of perfect fluids, J. Cosmol. Astropart. Phys. 03 (2021) 085.
[83] W. Yang, S. Pan, E. Di Valentino, O. Mena, and A. Melchiorri, 2021-H_0 odyssey: Closed, phantom and interacting dark energy cosmologies, J. Cosmol. Astropart. Phys. 10 (2021) 008.
[84] L.-Y. Gao, Z.-W. Zhao, S.-S. Xue, and X. Zhang, Relieving the H_0 tension with a new interacting dark energy model, J. Cosmol. Astropart. Phys. 07 (2021) 005.
[85] M. Lucca, Multi-interacting dark energy and its cosmological implications, Phys. Rev. D **104**, 083510 (2021).
[86] M. S. Linton, R. Crittenden, and A. Pourtsidou, Momentum transfer models of interacting dark energy, J. Cosmol. Astropart. Phys. 08 (2022) 075.
[87] R.-Y. Guo, L. Feng, T.-Y. Yao, and X.-Y. Chen, Exploration of interacting dynamical dark energy model with interaction term including the equation-of-state parameter: Alleviation of the H_0 tension, J. Cosmol. Astropart. Phys. 12 (2021) 036.
[88] S. Chatzidakis, A. Giacomini, P. G. L. Leach, G. Leon, A. Paliathanasis, and S. Pan, Interacting dark energy in curved FLRW spacetime from Weyl integrable spacetime, J. High Energy Astrophys. **36**, 141 (2022).
[89] R. G. Landim, Note on interacting holographic dark energy with a Hubble-scale cutoff, Phys. Rev. D **106**, 043527 (2022).
[90] Y. Zhao, Y. Liu, S. Liao, J. Zhang, X. Liu, and W. Du, Constraining interacting dark energy models with the halo concentration–mass relation, Mon. Not. R. Astron. Soc. **523**, 5962 (2023).
[91] L.-Y. Gao, S.-S. Xue, and X. Zhang, Dark energy and matter interacting scenario can relieve H_0 and S_8 tensions, arXiv:2212.13146.
[92] W.-T. Hou, J.-Z. Qi, T. Han, J.-F. Zhang, S. Cao, and X. Zhang, Prospects for constraining interacting dark energy models from gravitational wave and gamma ray burst joint observation, J. Cosmol. Astropart. Phys. 05 (2023) 017.
[93] Y. Zhai, W. Giarè, C. van de Bruck, E. Di Valentino, O. Mena, and R. C. Nunes, A consistent view of interacting dark energy from multiple CMB probes, J. Cosmol. Astropart. Phys. 07 (2023) 032.
[94] Y.-H. Li and X. Zhang, IDECAMB: An implementation of interacting dark energy cosmology in CAMB, J. Cosmol. Astropart. Phys. 09 (2023) 046.
[95] E. M. Teixeira, R. Daniel, N. Frusciante, and C. van de Bruck, Forecasts on interacting dark energy with standard sirens, Phys. Rev. D **108**, 084070 (2023).
[96] C. Rodriguez-Benites, M. Gonzalez-Espinoza, G. Otalora, and M. Alva-Morales, Revisiting the dynamics of interacting vector-like dark energy, arXiv:2311.02397.
[97] Y. L. Bolotin, A. Kostenko, O. A. Lemets, and D. A. Yerokhin, Cosmological evolution with interaction between dark energy and dark matter, Int. J. Mod. Phys. D **24**, 1530007 (2014).
[98] B. Wang, E. Abdalla, F. Atrio-Barandela, and D. Pavon, Dark matter and dark energy interactions: Theoretical challenges, cosmological implications and observational signatures, Rep. Prog. Phys. **79**, 096901 (2016).
[99] B. Wang, E. Abdalla, F. Atrio-Barandela, and D. Pavón, Further understanding the interaction between dark energy and dark matter: Current status and future directions, Rep. Prog. Phys. **87**, 036901 (2024).
[100] D. Pavon and W. Zimdahl, Holographic dark energy and cosmic coincidence, Phys. Lett. B **628**, 206 (2005).
[101] G. Huey and B. D. Wandelt, Interacting quintessence. The coincidence problem and cosmic acceleration, Phys. Rev. D **74**, 023519 (2006).
[102] S. del Campo, R. Herrera, and D. Pavon, Toward a solution of the coincidence problem, Phys. Rev. D **78**, 021302 (2008).
[103] S. del Campo, R. Herrera, and D. Pavon, Interacting models may be key to solve the cosmic coincidence problem, J. Cosmol. Astropart. Phys. 01 (2009) 020.
[104] B. Wang, Y.-g. Gong, and E. Abdalla, Transition of the dark energy equation of state in an interacting holographic dark energy model, Phys. Lett. B **624**, 141 (2005).
[105] H. M. Sadjadi and M. Honardoost, Thermodynamics second law and $\omega = -1$ crossing(s) in interacting holographic dark energy model, Phys. Lett. B **647**, 231 (2007).
[106] S. Pan and S. Chakraborty, A cosmographic analysis of holographic dark energy models, Int. J. Mod. Phys. D **23**, 1450092 (2014).
[107] S. Kumar and R. C. Nunes, Probing the interaction between dark matter and dark energy in the presence of massive neutrinos, Phys. Rev. D **94**, 123511 (2016).
[108] S. Kumar and R. C. Nunes, Echo of interactions in the dark sector, Phys. Rev. D **96**, 103511 (2017).
[109] S. Kumar, R. C. Nunes, and S. K. Yadav, Dark sector interaction: A remedy of the tensions between CMB and LSS data, Eur. Phys. J. C **79**, 576 (2019).
[110] N. Aghanim *et al.* (Planck Collaboration), Planck 2018 results. VI. Cosmological parameters, Astron. Astrophys. **641**, A6 (2020).
[111] A. G. Riess *et al.*, A comprehensive measurement of the local value of the Hubble constant with 1 km s^{-1} Mpc^{-1} uncertainty from the Hubble space telescope and the SH0ES team, Astrophys. J. Lett. **934**, L7 (2022).
[112] A. G. Riess, L. Breuval, W. Yuan, S. Casertano, L. M. Macri, J. B. Bowers, D. Scolnic, T. Cantat-Gaudin, R. I. Anderson, and M. C. Reyes, Cluster cepheids with high precision Gaia parallaxes, low zero-point uncertainties, and Hubble space telescope photometry, Astrophys. J. **938**, 36 (2022).
[113] A. Pourtsidou and T. Tram, Reconciling CMB and structure growth measurements with dark energy interactions, Phys. Rev. D **94**, 043518 (2016).
[114] R. An, C. Feng, and B. Wang, Relieving the tension between weak lensing and cosmic microwave background with interacting dark matter and dark energy models, J. Cosmol. Astropart. Phys. 02 (2018) 038.
[115] M. Asgari *et al.*, KiDS + VIKING-450 and DES-Y1 combined: Mitigating baryon feedback uncertainty with COSEBIs, Astron. Astrophys. **634**, A127 (2020).
[116] M. Asgari *et al.* (KiDS Collaboration), KiDS-1000 cosmology: Cosmic shear constraints and comparison

between two point statistics, Astron. Astrophys. **645**, A104 (2021).
[117] S. Joudaki *et al.*, KiDS+VIKING-450 and DES-Y1 combined: Cosmology with cosmic shear, Astron. Astrophys. **638**, L1 (2020).
[118] T. M. C. Abbott *et al.* (DES Collaboration), Dark Energy Survey Year 3 results: Cosmological constraints from galaxy clustering and weak lensing, Phys. Rev. D **105**, 023520 (2022).
[119] A. Amon *et al.* (DES Collaboration), Dark Energy Survey Year 3 results: Cosmology from cosmic shear and robustness to data calibration, Phys. Rev. D **105**, 023514 (2022).
[120] L. F. Secco *et al.* (DES Collaboration), Dark Energy Survey Year 3 results: Cosmology from cosmic shear and robustness to modeling uncertainty, Phys. Rev. D **105**, 023515 (2022).
[121] A. Loureiro *et al.* (KiDS and Euclid Collaborations), KiDS and Euclid: Cosmological implications of a pseudo angular power spectrum analysis of KiDS-1000 cosmic shear tomography, Astron. Astrophys. **665**, A56 (2022).
[122] C. Heymans *et al.*, KiDS-1000 cosmology: Multi-probe weak gravitational lensing and spectroscopic galaxy clustering constraints, Astron. Astrophys. **646**, A140 (2021).
[123] T. M. C. Abbott *et al.* (DES Collaboration), Dark Energy Survey Year 1 results: Cosmological constraints from cluster abundances and weak lensing, Phys. Rev. D **102**, 023509 (2020).
[124] O. H. E. Philcox and M. M. Ivanov, BOSS DR12 full-shape cosmology: ΛCDM constraints from the large-scale galaxy power spectrum and bispectrum monopole, Phys. Rev. D **105**, 043517 (2022).
[125] J. Gleyzes, D. Langlois, M. Mancarella, and F. Vernizzi, Effective theory of interacting dark energy, J. Cosmol. Astropart. Phys. 08 (2015) 054.
[126] C. G. Boehmer, N. Tamanini, and M. Wright, Interacting quintessence from a variational approach part I: Algebraic couplings, Phys. Rev. D **91**, 123002 (2015).
[127] C. G. Boehmer, N. Tamanini, and M. Wright, Interacting quintessence from a variational approach part II: Derivative couplings, Phys. Rev. D **91**, 123003 (2015).
[128] C. van de Bruck and J. Morrice, Disformal couplings and the dark sector of the universe, J. Cosmol. Astropart. Phys. 04 (2015) 036.
[129] G. D'Amico, T. Hamill, and N. Kaloper, Quantum field theory of interacting dark matter and dark energy: Dark monodromies, Phys. Rev. D **94**, 103526 (2016).
[130] W. Yang, S. Pan, L. Aresté Saló, and J. de Haro, Theoretical and observational bounds on some interacting vacuum energy scenarios, Phys. Rev. D **103**, 083520 (2021).
[131] A. Joseph and R. Saha, Forecast analysis on interacting dark energy models from future generation PICO and DESI missions, Mon. Not. R. Astron. Soc. **519**, 1809 (2022).
[132] L.-F. Wang, J.-H. Zhang, D.-Z. He, J.-F. Zhang, and X. Zhang, Constraints on interacting dark energy models from time-delay cosmography with seven lensed quasars, Mon. Not. R. Astron. Soc. **514**, 1433 (2022).
[133] H. Wei, Cosmological evolution of quintessence and phantom with a new type of interaction in dark sector, Nucl. Phys. **B845**, 381 (2011).
[134] H. Wei, Cosmological constraints on the sign-changeable interactions, Commun. Theor. Phys. **56**, 972 (2011).
[135] C.-Y. Sun and R.-H. Yue, New interaction between dark energy and dark matter changes sign during cosmological evolution, Phys. Rev. D **85**, 043010 (2012).
[136] Y.-H. Li and X. Zhang, Running coupling: Does the coupling between dark energy and dark matter change sign during the cosmological evolution?, Eur. Phys. J. C **71**, 1700 (2011).
[137] J.-J. Guo, J.-F. Zhang, Y.-H. Li, D.-Z. He, and X. Zhang, Probing the sign-changeable interaction between dark energy and dark matter with current observations, Sci. China Phys. Mech. Astron. **61**, 030011 (2018).
[138] F. Arevalo, A. Cid, L. P. Chimento, and P. Mella, On sign-changeable interaction in FLRW cosmology, Eur. Phys. J. C **79**, 355 (2019).
[139] S. Pan, W. Yang, C. Singha, and E. N. Saridakis, Observational constraints on sign-changeable interaction models and alleviation of the H_0 tension, Phys. Rev. D **100**, 083539 (2019).
[140] F. Arevalo and A. Cid, Dynamics and statefinder analysis of a class of sign-changeable interacting dark energy scenarios, Eur. Phys. J. C **82**, 946 (2022).
[141] L. A. Escamilla, O. Akarsu, E. Di Valentino, and J. A. Vazquez, Model-independent reconstruction of the interacting dark energy kernel: Binned and Gaussian process, J. Cosmol. Astropart. Phys. 11 (2023) 051.
[142] S. Pan, W. Yang, E. Di Valentino, D. F. Mota, and J. Silk, IWDM: The fate of an interacting non-cold dark matter—vacuum scenario, J. Cosmol. Astropart. Phys. 07 (2023) 064.
[143] R. Curbelo, T. Gonzalez, G. Leon, and I. Quiros, Interacting phantom energy and avoidance of the big rip singularity, Classical Quantum Gravity **23**, 1585 (2006).
[144] L. Amendola, M. Quartin, S. Tsujikawa, and I. Waga, Challenges for scaling cosmologies, Phys. Rev. D **74**, 023525 (2006).
[145] M. Quartin, M. O. Calvao, S. E. Joras, R. R. R. Reis, and I. Waga, Dark interactions and cosmological fine-tuning, J. Cosmol. Astropart. Phys. 05 (2008) 007.
[146] X.-m. Chen and Y. Gong, Fixed points in interacting dark energy models, Phys. Lett. B **675**, 9 (2009).
[147] X.-m. Chen, Y.-g. Gong, and E. N. Saridakis, Phase-space analysis of interacting phantom cosmology, J. Cosmol. Astropart. Phys. 04 (2009) 001.
[148] C. G. Boehmer, G. Caldera-Cabral, N. Chan, R. Lazkoz, and R. Maartens, Quintessence with quadratic coupling to dark matter, Phys. Rev. D **81**, 083003 (2010).
[149] N. Mahata and S. Chakraborty, Dynamical system analysis for DBI dark energy interacting with dark matter, Mod. Phys. Lett. A **30**, 1550009 (2015).
[150] M. Shahalam, S. D. Pathak, M. M. Verma, M. Y. Khlopov, and R. Myrzakulov, Dynamics of interacting quintessence, Eur. Phys. J. C **75**, 395 (2015).
[151] S. Singh and P. Singh, It's a dark, dark world: Background evolution of interacting ϕCDM models beyond simple

exponential potentials, J. Cosmol. Astropart. Phys. 05 (2016) 017.
[152] M. Khurshudyan and R. Myrzakulov, Phase space analysis of some interacting Chaplygin gas models, Eur. Phys. J. C **77**, 65 (2017).
[153] F. F. Bernardi and R. G. Landim, Coupled quintessence and the impossibility of an interaction: A dynamical analysis study, Eur. Phys. J. C **77**, 290 (2017).
[154] S. Carneiro and H. A. Borges, Dynamical system analysis of interacting models, Gen. Relativ. Gravit. **50**, 129 (2018).
[155] M. Shahalam, S. D. Pathak, S. Li, R. Myrzakulov, and A. Wang, Dynamics of coupled phantom and tachyon fields, Eur. Phys. J. C **77**, 686 (2017).
[156] S. D. Odintsov and V. K. Oikonomou, Study of finite-time singularities of loop quantum cosmology interacting multifluids, Phys. Rev. D **97**, 124042 (2018).
[157] M. Aljaf, D. Gregoris, and M. Khurshudyan, Phase space analysis and singularity classification for linearly interacting dark energy models, Eur. Phys. J. C **80**, 112 (2020).
[158] A. Paliathanasis, S. Pan, and W. Yang, Dynamics of nonlinear interacting dark energy models, Int. J. Mod. Phys. D **28**, 1950161 (2019).
[159] A. Hernández-Almada, M. A. García-Aspeitia, J. Magaña, and V. Motta, Stability analysis and constraints on interacting viscous cosmology, Phys. Rev. D **101**, 063516 (2020).
[160] C. Kaeonikhom, P. Rangdee, H. Assadullahi, B. Gumjudpai, J. A. Schewtschenko, and D. Wands, Qualitative dynamics of interacting vacuum cosmologies, Phys. Rev. D **102**, 123519 (2020).
[161] S. K. Biswas and A. Biswas, Phase space analysis and thermodynamics of interacting Umami Chaplygin gas in FRW universe, Eur. Phys. J. C **81**, 356 (2021).
[162] S. Chakraborty, S. Mishra, and S. Chakraborty, A dynamical system analysis of cosmic evolution with coupled phantom dark energy with dark matter, Int. J. Mod. Phys. D **31**, 2150129 (2022).
[163] P. M. Sá, Late-time evolution of the Universe within a two-scalar-field cosmological model, Phys. Rev. D **103**, 123517 (2021).
[164] W. Khyllep, J. Dutta, S. Basilakos, and E. N. Saridakis, Background evolution and growth of structures in interacting dark energy scenarios through dynamical system analysis, Phys. Rev. D **105**, 043511 (2022).
[165] P. M. Sá, Coupled quintessence inspired by warm inflation, arXiv:2312.09171.
[166] S. Bahamonde, C. G. Böhmer, S. Carloni, E. J. Copeland, W. Fang, and N. Tamanini, Dynamical systems applied to cosmology: Dark energy and modified gravity, Phys. Rep. **775–777**, 1 (2018).
[167] S. Nojiri, S. D. Odintsov, and S. Tsujikawa, Properties of singularities in (phantom) dark energy universe, Phys. Rev. D **71**, 063004 (2005).
[168] S. Nojiri and S. D. Odintsov, Inhomogeneous equation of state of the universe: Phantom era, future singularity and crossing the phantom barrier, Phys. Rev. D **72**, 023003 (2005).
[169] T. M. Apostol, *Mathematical Analysis*; 2nd ed., Addison-Wesley Series in Mathematics (Addison-Wesley, Reading, MA, 1974).